NASA CR-114479

STUDY OF SPRAY DISINTEGRATION IN ACCELERATING FLOW FIELDS

By W. H. Nurick

June 1972

Prepared under Contract No. NAS2-6494 by
Rocketdyne/North American Rockwell Corporation
Canoga Park, California

for

Jet Propulsion Laboratory
National Aeronautics and Space Administration
Pasadena, California

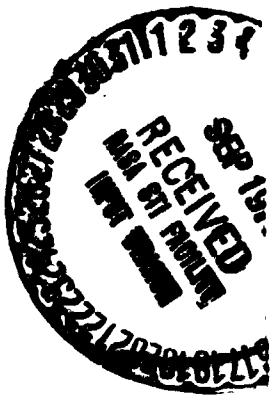

NASA CR-114479

STUDY OF SPRAY DISINTEGRATION IN ACCELERATING FLOW FIELDS

June 1972

Contract No. NAS2-6494

W. H. Nurick

APPROVED BY

L. P. Combs
Manager

Rocketdyne
North American Rockwell

6633 Canoga Avenue,
Canoga Park, California 91304

PRECEDING PAGE BLANK NOT FILMED

ACKNOWLEDGEMENT

Important contributions to the Combustion Model Analysis portion of this program were made by W. D. Chadwick of the Advanced Programs Division.

FOREWORD

The work described herein was conducted by Rocketdyne, a Division of North American Rockwell Corporation, in accordance with the terms of Contract NAS2-6494 for the National Aeronautics and Space Administration, Jet Propulsion Laboratory, Pasadena, California. Mr. R. M. Clayton of the Jet Propulsion Laboratory served as the NASA Technical Manager. The Rocketdyne Program Manager was Mr. L. P. Combs. Technical guidance of the program was provided by Dr. D. T. Campbell.

This report has been designated Rocketdyne Report No. R-9017.

ABSTRACT

An analytical and experimental investigation was conducted to perform "proof of principle" experiments to establish the effects of propellant combustion gas velocity on propellant atomization characteristics. The propellants were gaseous oxygen (GOX) and Shell Wax 270. The fuel was thus the same fluid used in earlier primary cold-flow atomization studies using the frozen wax method. Experiments were conducted over a range in L* (30 to 160 inches) at two contraction ratios (2 and 6). Characteristic exhaust velocity (c*) efficiencies varied from 50 to 90 percent. The hot fire experimental performance characteristics at a contraction ratio of 6.0 in conjunction with analytical predictions from the droplet heat-up version of the Distributed Energy Release (DER) combustion computer program showed that the apparent initial dropsize compared well with cold-flow predictions (if adjusted for the gas velocity effects). The results also compared very well with the trend in performance as predicted with the model. Significant propellant wall impingement at the contraction ratio of 2.0 precluded complete evaluation of the effect of gross changes in combustion gas velocity on spray dropsize.

CONTENTS

ILLUSTRATIONS

TABLES

SUMMARY

An analytical and experimental investigation was conducted to perform "proof of principle" experiments to establish the effects of propellant combustion gas velocity on propellant atomization characteristics. The overall study was divided into several steps. The first step involved theoretical performance analysis to define combustor operating characteristics as functions of mixture ratio. The second step was hardware design and fabrication, which encompassed the design of the injector as well as a solid wall combustion chamber/nozzle assembly. In the third step, hot-fire experiments were conducted to determine c* efficiency characteristics as functions of chamber length for two differing contraction ratios (2 and 6). Lastly (step 4), analysis of results combined with combustion model analysis were accomplished to determine whether or not combustion gas velocity significantly affected the initial injected spray dropsize and promoted secondary droplet breakup.

The propellants were gaseous oxygen (GOX) and Shell Wax 270. The fuel selected (wax) was the same fluid used in earlier primary cold-flow atomization studies using the frozen wax technique. Experiments were conducted over a range in L* (30 to 160 inches) at two contraction ratios (2 and 6). Characteristic exhaust velocity (c*) efficiencies (corrected for heat loss) varied from 50 to 90 percent. The hot-fire experimental performance characteristics at a contraction ratio of 6, in conjunction with analytical predictions from the droplet heat-up version of the Distributed Energy Release (DER) computer program, showed that the apparent initial dropsize compared well with cold-flow predictions (if adjusted for the gas velocity effects). The results also compared very well with the trend in performance as predicted with the model for constant initial dropsize. Significant propellant wall impingement at the contraction ratio of 2 precluded evaluating the effects of changes in gas velocity on dropsize. The results therefore provided a reasonable first check on the combustion model but unfortunately, due to spray impinging on the chamber wall at contraction ratio of 2, the results neither confirmed nor denied the basic premises that secondary

spray droplet breakup is effected by the accelerating combustion gases and that the extent of breakup depends upon the relative gas velocity level. This experimental defect was disappointing since the experimental method is ideally suited to this important determination. The technical problem areas are discussed in the body of the report and techniques for their avoidance are suggested.

INTRODUCTION

Over the past several years, analytical models describing liquid rocket engine combustion processes have been significantly improved. These models require as input the propellant mass flux and mixture ratio distribution as well as the spray dropsize distributions. Such data are commonly acquired by cold-flow injection modeling techniques using simulant fluids. For example, mass and mixture ratio distributions for liquid/liquid propellant combinations are generally measured using immiscible fluids such as water/trichloroethylene or water/carbon tetrachloride and, for measurement of dropsize distributions, a considerable amount of data have been generated using molten wax as a liquid propellant simulant. Measurements made in nonreactive experiments using simulant propellants must be corrected for the effects of differing propellant physical properties and the environment occurring in the rocket engine before being input into mixing and vaporization rate-limited combustion models.

Excellent agreement between mixing-limited combustion efficiency predicted from using combustion models, cold-flow data, and actual hot-fire results has been found and is reported in Ref. 1 and 2. While vaporization-limited performance predictions based upon these models have generally been successful in predicting trends, especially the effects of variations in chamber length, it has, however, often been necessary to adjust input dropsizes for effects of chamber contraction area ratio (combustion gas velocity) and physical properties to correlate empirically vaporization-limited experimental hot-firing results with combustion model predictions (Ref. 3). This uncertainty in relating actual propellant spray mean dropsizes obtained under firing conditions to cold-flow correlations is probably the greatest remaining weakness in liquid rocket engine performance analysis.

Considerable evidence has suggested that the discrepancies between cold-flow mean dropsizes and apparent mean dropsizes based on hot-firing performance data is indeed attributable to (1) the influences of combustion gas shear forces, both during initial spray formation and subsequent aerodynamic breakup of droplets or "secondary breakup" and (2) to differing physical properties between

simulant fluids and actual propellants. If these parameters do affect the atomization (both primary and secondary) in liquid rocket engines, then a thorough experimental evaluation of their characteristics would be warranted. The objective of this study has been to conduct a series of critical "proof of principle" hot-firing experiments to show, unequivocally, the influence of changing combustion gas velocity levels on apparent mean dropsize (based on performance). In addition, data obtained were expected to provide the basis for realistic cold-flow modeling criteria and indicate whether or not cold-flow simulation of the overall atomization process is appropriate. To eliminate the need of a physical property correction, Shell Wax 270 was selected as the fuel propellant since dropsize correlations have been obtained using this particular wax. Gaseous oxygen was selected as the oxidizer to avoid bipropellant dropsizes and the need for dropsize correlations with another fluid. The results from this study are presented.

PROPELLANTS SELECTION AND C* PERFORMANCE CHARACTERISTICS

PROPELLANTS SELECTION

The major factors affecting the choice of propellants are related to using combustion model performance predictions in conjunction with experimental results to determine the influence of combustion gas velocity on dropsize. In particular, this technical approach is totally dependent on the validity of the combustion model formulation. Unfortunately the vaporization aspects of the combustion models themselves have never been adequately verified since known propellant spray dropsizes from actual injectors have not been available as input for comparison with actual hot-fire data. In the past, these models have been used to predict the dropsizes that must have been present to obtain the resultant combustion performance. These combustion model predictions invariably resulted in dropsizes considerably smaller than those predicted from dropsize correlations developed using other fluids. Consequently, verification of the models could not be accomplished.

For this study, it was decided to select propellants for which dropsize correlations had been developed in order that the initial spray dropsizes would be known. In this way, the actual level of dropsize obtained by comparison of combustion model predictions with the hot fire results could be compared with that predicted from independent dropsize correlations. In addition, using this approach would not require the use of physical property corrections that have not been adequately verified to "artificially" correct the dropsize determined using empirical correlations that were developed using fluids with differing physical properties. Consequently, direct check on the validity of the model formulation could be obtained under combustion conditions where secondary breakup is not likely to occur. A second factor affecting the selection of the propellants is to avoid reactive stream separation which, if it occurred, would invalidate the approach. To ensure avoidance of this problem area, all hypergolic propellant combinations were rejected from consideration. Lastly, not to complicate the dropsize predictions, it was also desirable to have only one propellant injected as a liquid. This avoids the problem of bipropellant vaporization.

Based upon the above-described considerations, Shell Wax 270 was selected as the fuel and gaseous oxygen was selected as the oxidizer. Shell Wax 270 was selected because a considerable quantity of experimental data has been obtained relating dropsize to injector mechanical and hydraulic parameters (e.g., Ref. 1 through 4). Consequently, empirical correlations are available. Gaseous oxygen provides both a nonhypergolic propellant combination and a gaseous propellant so that only the vaporization of the fuel need be considered in the combustion model.

As will be discussed later in the report, selection of these propellants, while meeting all of the above requirements, did result in one serious defect. This defect was that the time required for the wax droplets to reach their boiling temperature was excessive when injected into the chamber at a nominal temperature of 200 F, which was the experimental approach used. This condition resulted in excessive wall impingement of the wax under some conditions because insufficient gas velocity was generated in the initial combustion region to turn the wax spray in the axial direction.

THEORETICAL PERFORMANCE ANALYSIS

The Rocketdyne theoretical performance model was utilized to generate theoretical c* and combustion gas temperature for the propellants gaseous oxygen/Shell wax 270. The assumed operating conditions were $0.1 \leq MR \leq 20$, a chamber pressure of 50 psia, and an initial propellant temperature of 200 F. All pertinent thermochemical data for the wax necessary for this analysis were obtained from the Shell Oil Company. The results are presented in Fig. 1 for both full shifting characteristic velocity (c*) and stagnation temperature as a function of mixture ratio. Note that the optimum c* occurs at a mixture ratio of 2.0, while the maximum equilibrium temperature occurs at a mixture ratio of about 3.0. Based upon these calculations, a mixture ratio of 2.0 was selected for the design operating point. At this mixture ratio, the values of c* and T_c are:

$$\left.\begin{aligned} P_c &= 50 \text{ psia} \\ c^* &= 5877 \text{ ft/sec} \\ T_o &= 2640 \text{ F} \end{aligned}\right\} \quad \text{at MR} = 2.0$$

A summary of the combustion gas properties at the above conditions are presented below:

$C_{p_{frozen}}$	= 0.511 cal/gm-K
$Gamma_{frozen}$	= 1.241
Viscosity	= 0.0868 centipoise (0.2101 lb/hr-ft)
Thermal Conductivity (k)	= 0.1334 Btu/hr-ft-F
Molecular weight	= 20.018

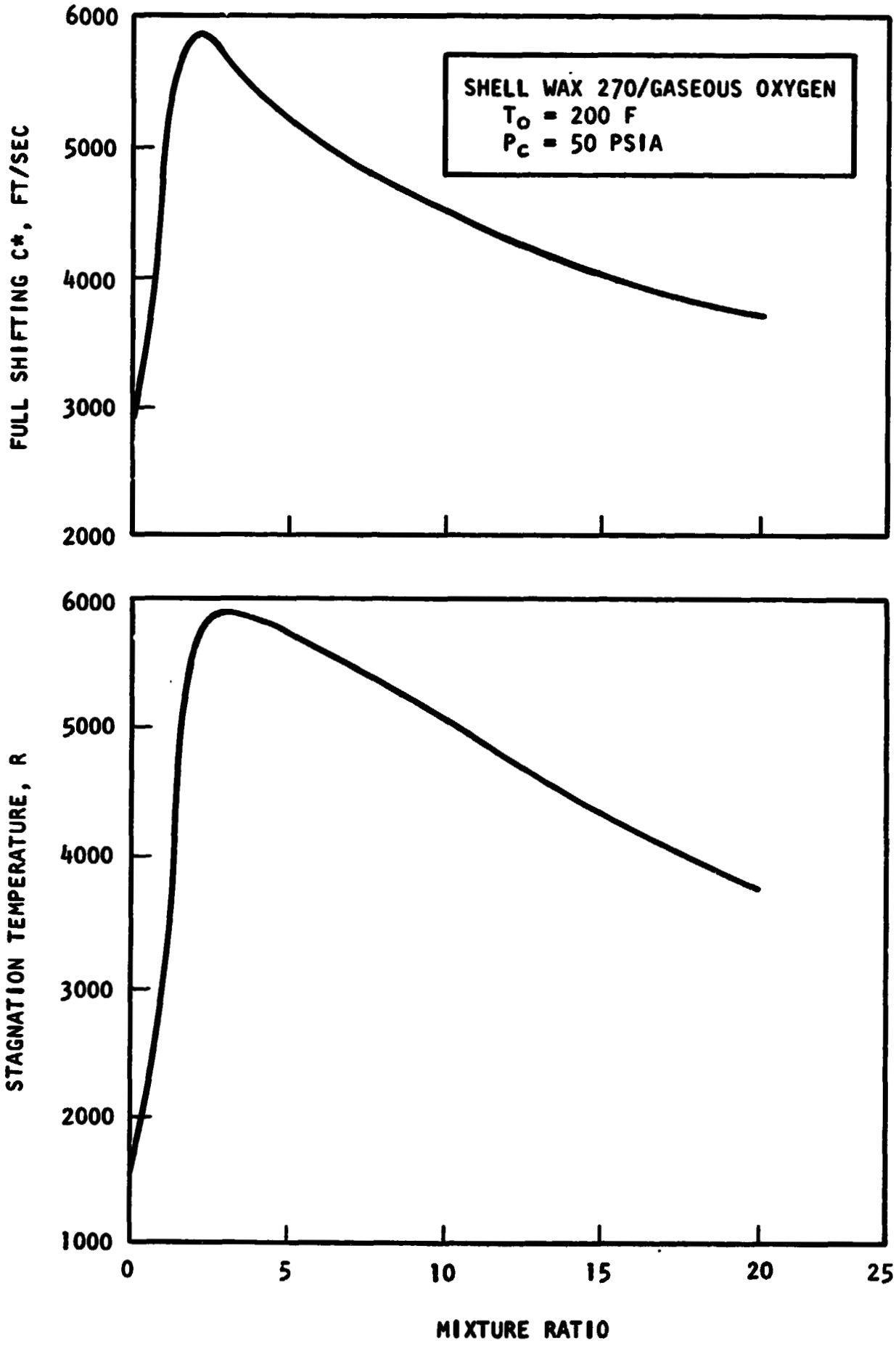

Figure 1. Theoretical Equilibrium Calculation for Combustion of Shell Wax 270/GOX

HARDWARE DESIGN ANALYSIS AND SPECIFICATION

The design of a rocket engine injector and chamber requires specification of engine operating conditions, as well as physical and thermal properties. This section contains descriptions of the results of (1) determination of physical properties for the wax (GOX data are readily available in the literature), and (2) injector/chamber design, which includes a simplified combustion analysis to select the overall chamber length required to obtain nearly complete combustion and a heat transfer analysis to define chamber materials as well as firing duration.

The selected operating conditions for design are:

P_c = 50 psia

MR = 2.0

SHELL WAX 270 PHYSICAL PROPERTIES

A summary of physical property data furnished by the Shell Chemical Company or estimated from homologous series straight-chain paraffin data are presented in Table 1. The values are given at a wax temperature of 200 F.

TABLE 1. SHELL WAX 270 PHYSICAL PROPERTIES

Boiling Point** at 50 psia, F	ΔH_v at Saturation Temperature*, Btu/lb	Density** lbm/ft^3	Viscosity lbm/ft-sec	Surface Tension** dynes/cm
1525	40 (approx.)	47.7	2.69×10^{-3}	17

*Properties evaluated at 200 F
**Estimated

The effect of temperature on viscosity and surface tension are presented in Fig. 2a and 2b. It is interesting to compare these physical-properties data with those of the "normal" fuel propellants shown below in Table 2.

TABLE 2. PHYSICAL-PROPERTIES OF SEVERAL NORMAL FUEL PROPELLANTS

Fuel	Boiling Point, F	ΔH_v at Saturation Temperature Btu/lb	Density lbm/ft^3	Viscosity, lbm/ft-sec	Surface Tension dynes/cm
Hydrazine	236.3	540.0	58.6	0.625×10^{-3}	67
50-50	170.0	425.8	55.5	0.55×10^{-3}	47*
RP-1	422	125.0	49.2	1.04×10^{-3}	23

*Estimated

Comparison of the boiling temperatures for the various fuels shows that the wax boiling temperature is 1000 to 1200 degrees higher than that of the normal fuels. This difference suggests that there may be considerable time required for the wax to be heated from its injection temperature to its boiling temperature. Also note that the latent heat of vaporization (ΔH_v) is considerably less for the wax than the others. This shows that once vaporization is initiated, the wax requires considerably less heat energy to vaporize than the other fuels listed. The viscosity and surface tension should only affect the initial droplet size. The surface tension for the wax is lower than that of the other fuels while the viscosity is 1 to 5 times greater. These differences suggest that, for the same flow energy, the wax would result in larger drop sizes than the other fuels (Ref. 1).

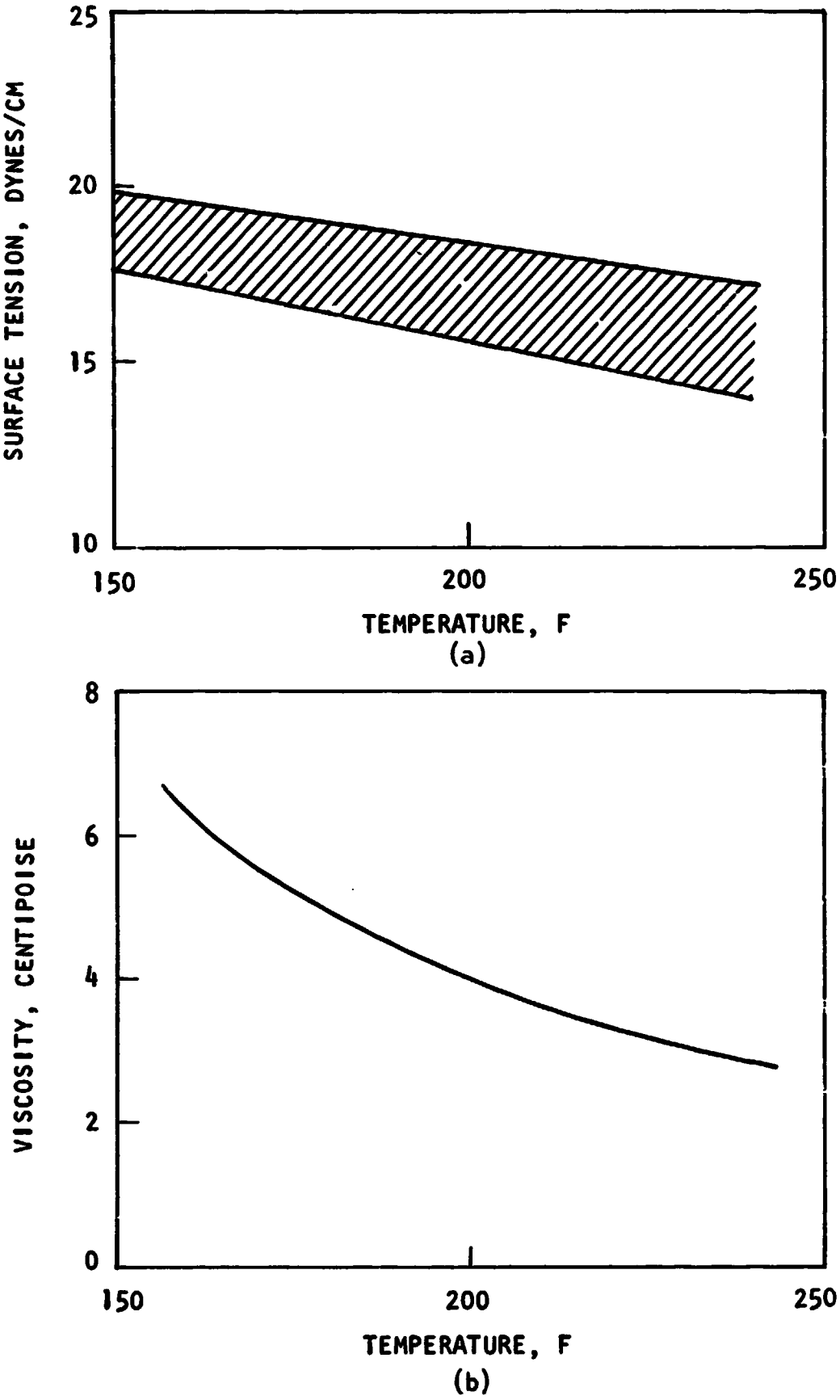

Figure 2. The Effect of Temperature on Viscosity and Surface Tension for Shell Wax 270

HARDWARE DESIGN

The hardware for this program consists of a single-element like-doublet (molten wax) injector with a Rigimesh face plate for injection of gaseous oxygen and four solid wall rectangular chambers of differing lengths, each with adaptors for two contraction ratios (2.0 and 6.0). The overall requirements and the rationale for selection of the specific dimensions and injection conditions are discussed below.

INJECTOR DESIGN

P_c = 50 psia
MR = 2.0 (specified from theoretical combustion analysis)

The resulting flowrates based on 100 percent c* efficiency are:

$$w_f = \frac{1.095}{3} = 0.365 \text{ lb/sec}$$

$$w_o = 1.095 - 0.365 = 0.730 \text{ lb/sec}$$

Wax Doublet

The overall range in orifice size, for like-impinging doublet elements, studied under the NAS7-726 contract (Ref. 4) was 0.062 to 0.081 inch. A requirement for this contract was to utilize an element diameter size within the range covered under NAS7-726. Based upon the design operating values and expected drop sizes, an orifice size of 0.069-inch was selected. The injector consists of an orifice L/D of 100, free-stream impingement L/D of 5.0, and included impingement angle of 60 degrees.

The discharge coefficient for an orifice of L/D = 100, D_j = 0.069-inch flowing heated wax, and having a rounded entrance was determined using the results of the single orifice study of Ref. 4. The resulting discharge coefficient

(including friction) is presented in Fig. 3a as a function of injection velocity. The corresponding orifice ΔP characteristics are shown in Fig. 3b.

Based on the flowrate requirements specified above, the orifice injection velocity and ΔP at the design operating conditions are:

$$V_j = 148 \text{ ft/sec}$$

$$\Delta P = 400 \text{ psi}$$

Gaseous Oxygen Face Plate

A Rigimesh face plate was used to inject the gaseous oxygen into the combustion chamber. This design provides sufficiently uniform dispersion of the oxygen such that the effective flow area is the chamber cross-section. The specification for the Rigimesh is 400 psi pressure drop at a flowrate of 0.730 lb/sec. The gas velocities near the injector face assuming rapid expansion to the chamber cross sectional dimensions are:

$$V_g = 19.4 \text{ ft/sec at } \varepsilon_c = 6.0$$

$$V_g = 58.3 \text{ ft/sec at } \varepsilon_c = 2.0$$

A summary of the injector design parameters is given in Table 3.

TABLE 3. SUMMARY OF INJECTOR DESIGN PARAMETERS

ε_c	V_{wax}, ft/sec	D_{wax}, inch	V_{ox}, ft/sec	θ, deg	$(L/D)_{Orifice}$	$(L/D)_{Free\ Stream}$
2.0	148	0.069	58.3	60	100	5
6.0	148	0.069	19.4	60	100	5

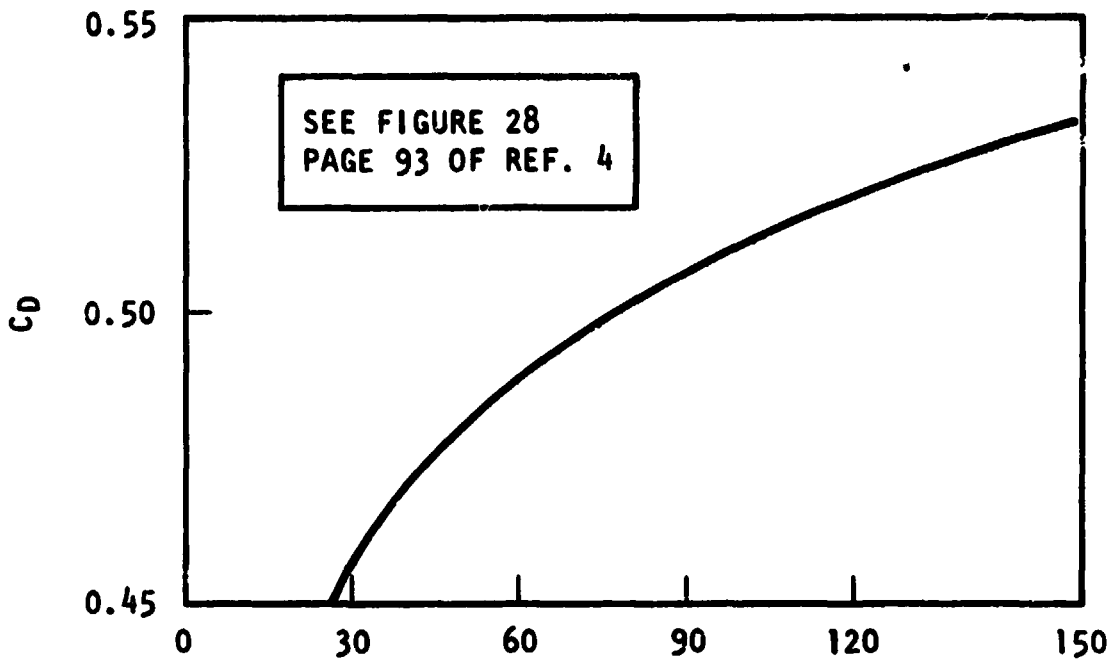

a. DISCHARGE COEFFICIENT CHARACTERISTICS

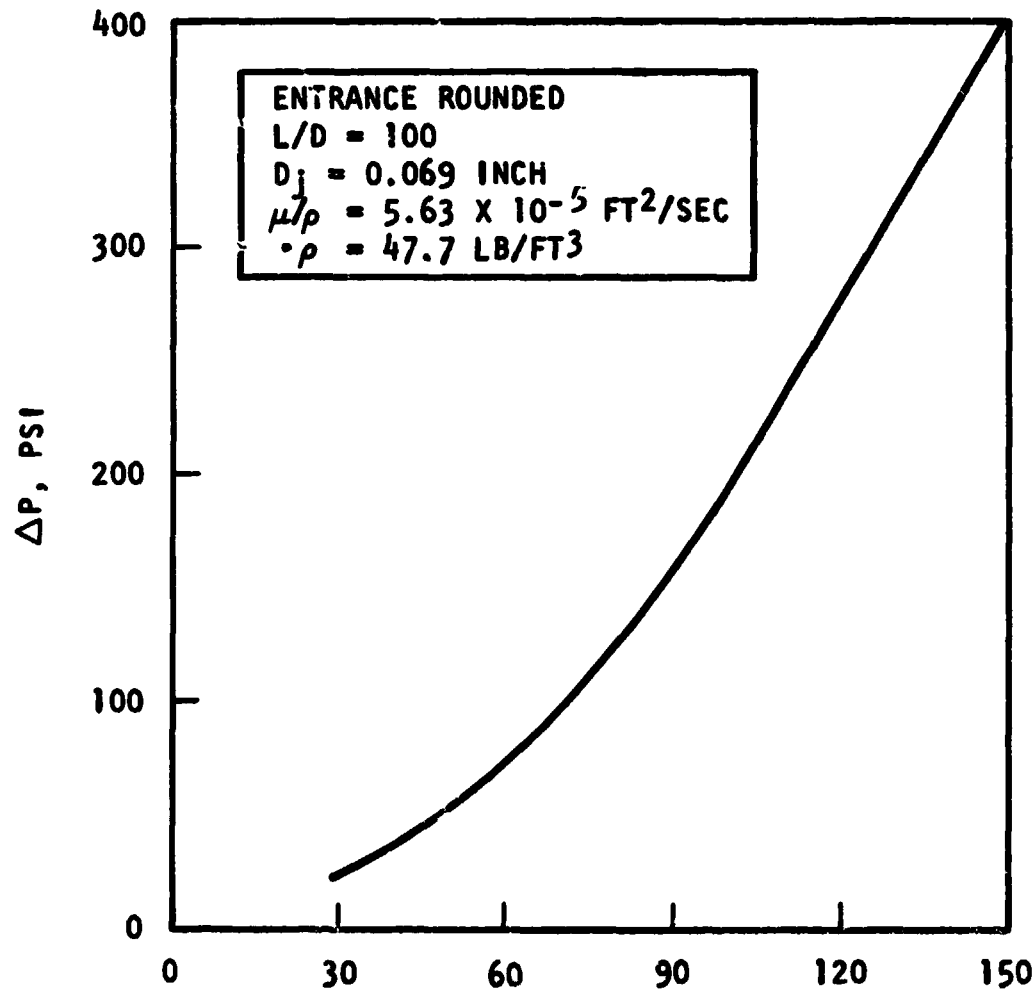

b. ORIFICE PRESSURE DROP CHARACTERISTICS

Figure 3. Orifice Flow Characteristics Using Shell Wax 270

A schematic view of the resulting injector design is shown on Fig. 4. Note that a tube is provided between the two wax jets; this tube flows F_2 gas for ignition.

Checkout experiments revealed that the Rigimesh face plate resulted in choked flow, which in turn unchoked the GOX venturi. To eliminate this problem, small holes (0.029 inch) were drilled through the face plate into the oxygen manifold. The holes were along the periphery of the plate and several holes were drilled along the larger dimension centerline. This provided sufficient additional injection flow area that the flow was then controlled by sonic flow at the GOX venturi.

THRUST CHAMBER/NOZZLE DESIGN

The minimum chamber cross-sectional dimensions were dictated by the spray fan geometry and the maximum chamber length was defined by the length required to obtain nearly complete vaporization of the wax. The materials selected and firing duration were specified from heat transfer considerations.

SPECIFICATION OF CHAMBER CROSS SECTIONAL DIMENSIONS

Several runs were made of the Liquid Injector Spray (LISP) computer program (Ref. 5) assuming zero gas velocity, to obtain the mass flux profiles at differing axial distances of the spray emanating from a like-impinging doublet. The results showed that the minimum chamber cross-sectional dimensions should be between 6 to 8 inches along the long axis of the fan and 2 to 3 inches along the other dimension (edge of the fan). Since the gas velocity was assumed to be zero, these dimensions apply to the contraction ratio of 6.0 configuration. It would be expected that the higher gas velocities at a contraction ratio of 2.0 would turn the fan earlier and thereby reduce the required dimensions of the spray field.

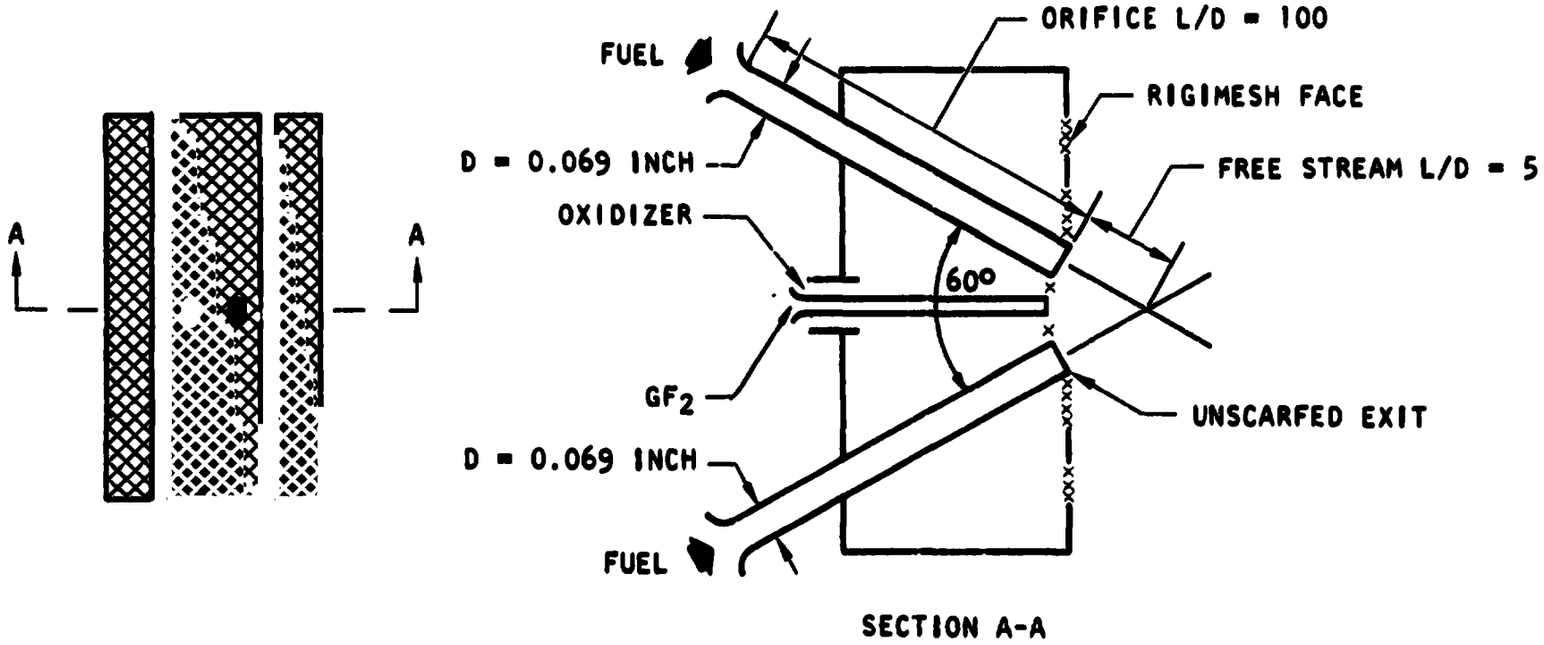

Figure 4. Schematic of Injector Configuration

Two-dimensional throat geometry that would taper in only one plane was selected. For a two-dimensional throat and for a contraction ratio of 2.0 the chamber dimensions are:

$$A_c/A_t = \frac{L_c\ W_c}{L_t\ W_t} = 2.0 \qquad (1)$$

A = area
L = length
W = width
c,t= chamber, and throat respectively

and if $L_c = L_t$, then $W_c = 2.0\ W_t$

In addition,

$$L_t\ W_t = A_t = L_c\ W_t \qquad (2)$$

Both Eq. 1 and 2 are shown plotted on Fig. 5. The limits shown by the upper shaded area are the result of the calculated spray mass flux profile (6 to 8-inches) while the lower shaded area limit is a minimum width of 1.0 inch. The remaining region which lies within these bounds is shown by the dark area on Fig. 5. A design that falls within the design range was selected; the dimensions are:

$L_t = L_c = 7.0$ inches
$W_c = 1.15$ inches
$W_t = 0.57$ inch
$\varepsilon_c = 2.0$

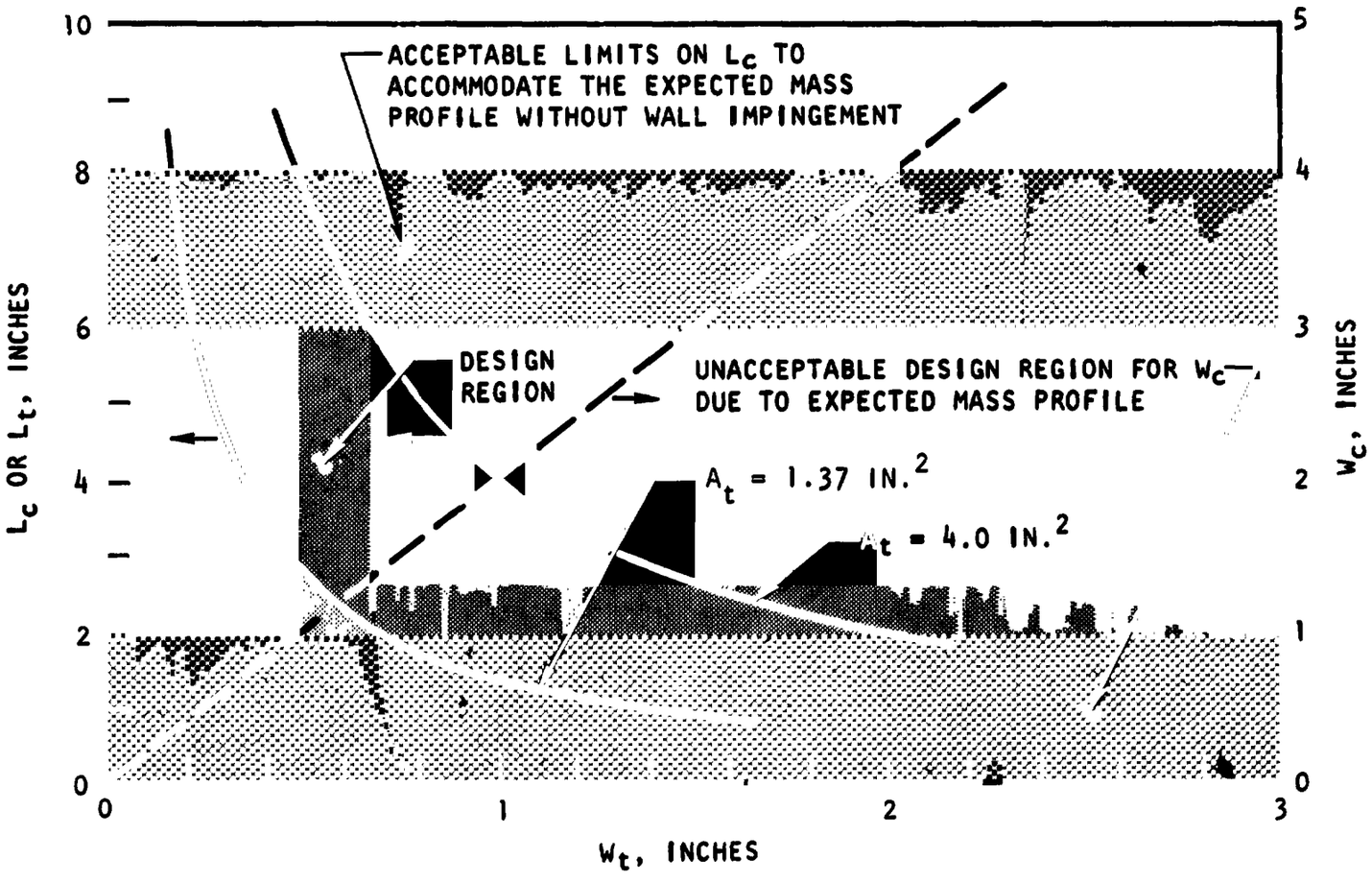

Figure 5. Design Curve for 2-Dimensional Throat Geometry at a Chamber Contraction Ratio of 2.0 ($L_c = L_t$)

Based on these values at a contraction ratio of 2.0, the corresponding chamber dimensions for a contraction ratio of 6.0 are:

L_c = 7.0 inches

W_c = 3.45 inches

These values are within the acceptable design range dictated by the mass fiux profile generated using the LISP program.

SPECIFICATION OF CHAMBER LENGTH

To determine experimentally the mixing efficiency of the engine, the chamber length must be sufficiently long to ensure complete spray evaporation and com bustion. To aid in rational selection of the required chamber length, the Rocketdyne-developed DER program (without droplet heating) was used to predict the vaporization characteristics as a function of chamber length. The DER (without droplet heating) program was run in a single-stream tube mode (i.e., assuming uniform mixing).

Analysis of the effect of chamber length on vaporization efficiency showed that for a contraction ratio of 2.0, a chamber length of 15 inches should be sufficient to obtain 99 percent c* efficiency.

HEAT TRANSFER ANALYSIS

To obtain steady-state flow conditions during a test, a minimum of 3 seconds firing duration is desirable. For the specific operating conditions listed above, transient gas-side wall temperature histories were calculated for the nozzle throat. Calculations were performe for several possible wall materials (OFHC, 347 RES, and mild steel). The gas-side heat transfer coefficient was calculated from the correlation given in Ref. 6. A value for h_g of 0.00061 Btu/in.^{2}-sec-F was used. The results of the transient analysis are presented in Fig. 6.

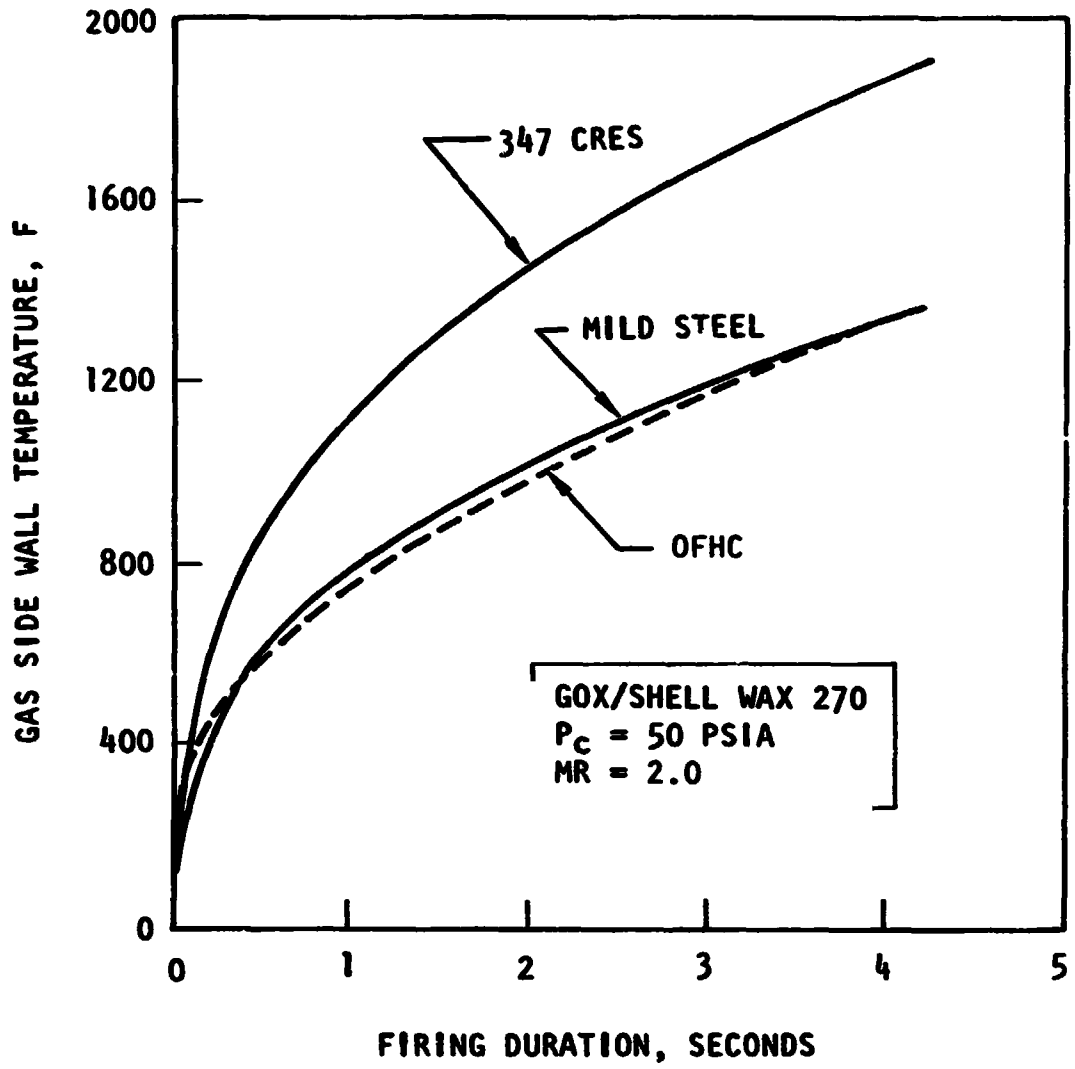

Figure 6. Effect of Wall Material on the Transient Temperature Response of the Gas Side Wall

Review of the temperature histories after 3 seconds of test duration indicates that both the OFHC copper and the mild steel materials were attractive as the chamber wall material. Based upon the calculations presented in Fig. 6, OFHC was selected as the throat material as an added margin of safety while mild steel was selected for the chamber material due to its low cost.

INJECTOR/THRUST CHAMBER DESIGNS

The preceding analyses were used to specify the overall dimensions for the injector and thrust chamber/nozzle assembly. Based upon these specifications, the injector/thrust chamber designs shown in Fig. 7 and 8 were specified. As shown in Fig. 7, the overall chamber is designed such that length extensions are obtained by simply adding sections. Chamber sections were designed to provide overall assembled lengths (injector to beginning of contraction) of 6, 10.7, 15, 24, 30, and 39 inches.

More detail of the injector and chamber inserts for reduction in contraction ratio is shown in Fig. 8. Note that the wall near the injector tapers from the design condition of contraction ratio of 6.0 to the value of 2.0. This was necessary since the injector ΔP across Rigimesh face is prohibitively large if the flow area is reduced. In addition, a reduction would require special seals that would increase fabrication costs. This design feature presented no problems since the velocities in the chamber near the injector are low (see prior calculations). For the contraction ratio of 2.0, the initial tapered section of the nozzle is removed so that a smooth transition (without a setup) occurs between the chamber and nozzle. A complete summary of the chamber dimensions is presented in Tables 4 and 5.

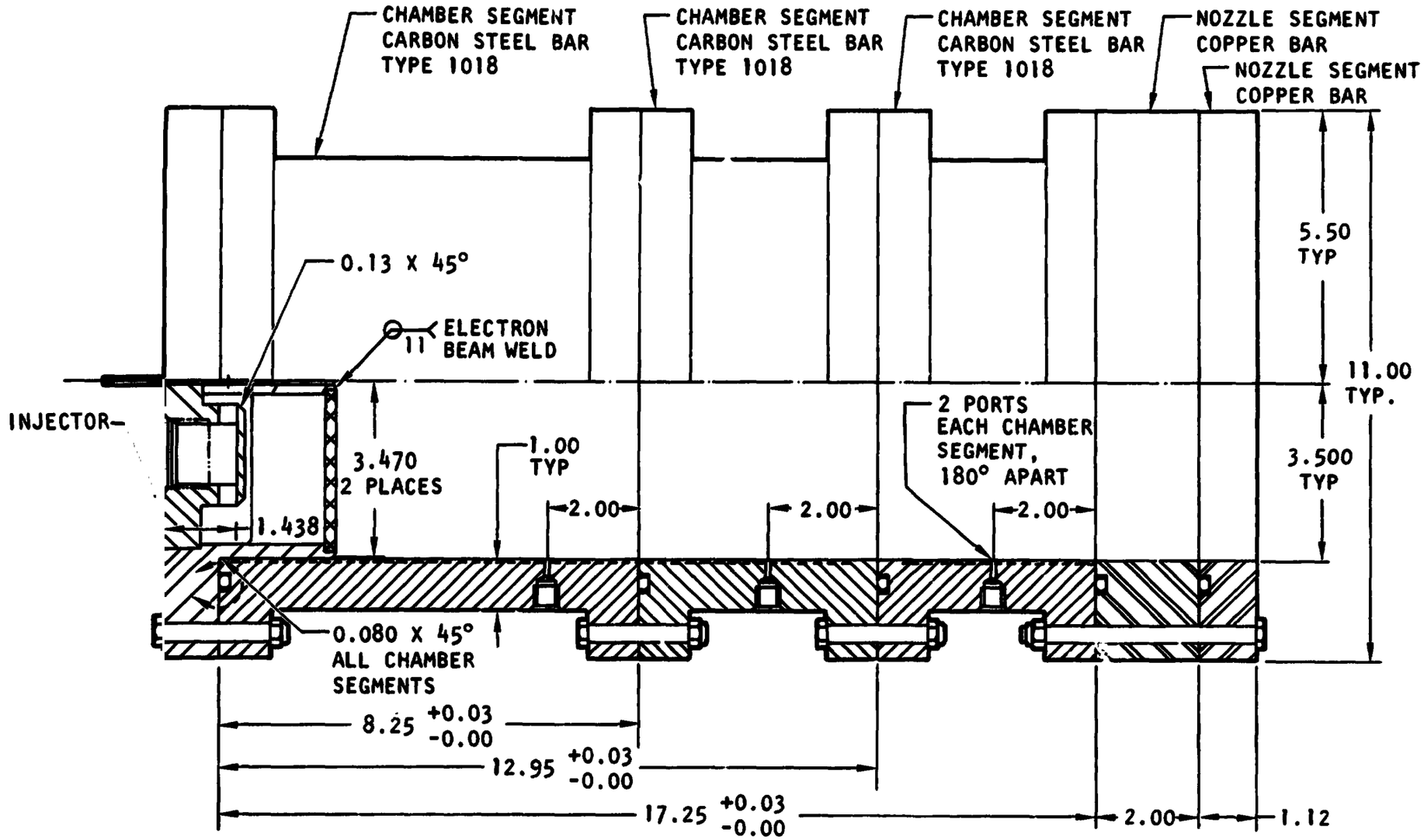

Figure 7. Overall Assembly of Test Engine

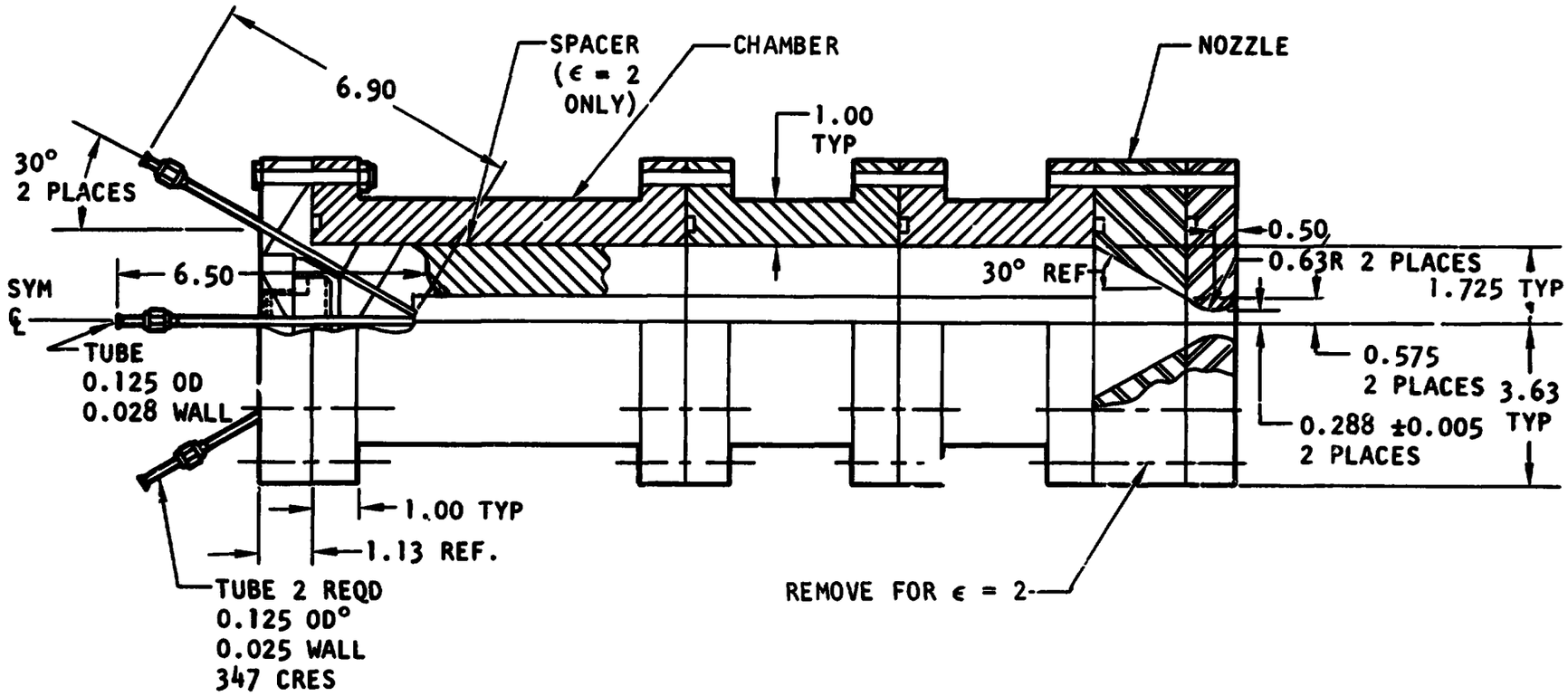

Figure 8. Overall Assembly of Test Engine, Injector and Nozzle Assembly

TABLE 4. SUMMARY OF CHAMBER CROSS-SECTIONAL DIMENSIONS

Contraction Ratio	Chamber		Throat	
ε_c	L_c, inch	W_c, inch	L_t, inch	W_t, inch
2.0	7.0	1.15	7.0	0.57
6.0	7.0	3.45	7.0	0.57

TABLE 5. SUMMARY OF CHAMRER AXIAL DIMENSIONS

Chamber Length*, inches	Chamber L*, inch	
	ε_c = 2	ε_t = 6
6	12.9	44.8
10.7	21.6	70.6
15	31.0	99.0
24	47.5	153.0
30	61.0	195.0
39	80.0	256.0

*Injector face to beginning of convergence

The chamber was designed for recording the chamber pressures near the beginning of convergence.

FACILITY AND INSTRUMENTATION

The testing was conducted on Zebra stand at the Propulsion Research Area. A schematic of the test stand is presented in Fig. 9. As shown, the wax and wax-purge (nitrogen gas) are preheated to about 200 F in a 55-gallon drum filled with boiling water. The water is heated by Kal-Rod heaters in the bottom of the drum. The hot wax purge is used to preheat the line from the main valve to the injector. This ensures that the wax will remain in the molten state as it flows through the lines to the injector. The heated wax purge gas is also used to force the wax out of the injector after firing. The gaseous oxygen propellant and the GOX purge are heated using a pebble bed heater to ensure that the entire injector manifold is sufficiently hot that the wax will not freeze in the injector.

The wax tank, which is immersed in the boiling water, is a 2-gallon, 2440-psia spherical tank. The entire line from the pressurizing valve to the inlet is jacketed. Since hot wax is aspirated into the pressurizing line during venting causing clogging, hot GN_2 from a separate heater source flows through the jacket to ensure that the wax will not freeze in the pressurizing line. The entire main line from the tank exit to the main valve is also immersed in the water tank.

Gaseous oxygen is supplied from a 76 K-bottle manifold. This ensures that there is sufficient oxygen for at least 40 runs without significant loss in bottle pressure. The line size to the injector is 1/2-inch.

Fluorine (gas) is used for ignition and is supplied from a K-bottle. This system is completely independent from the other systems.

Two flowmeters are used to measure the wax flowrates and a single sonic venturi is employed to determine the GOX flowrate. GOX inlet pressure and both fuel and oxidizer inlet temperatures are also measured. For performance

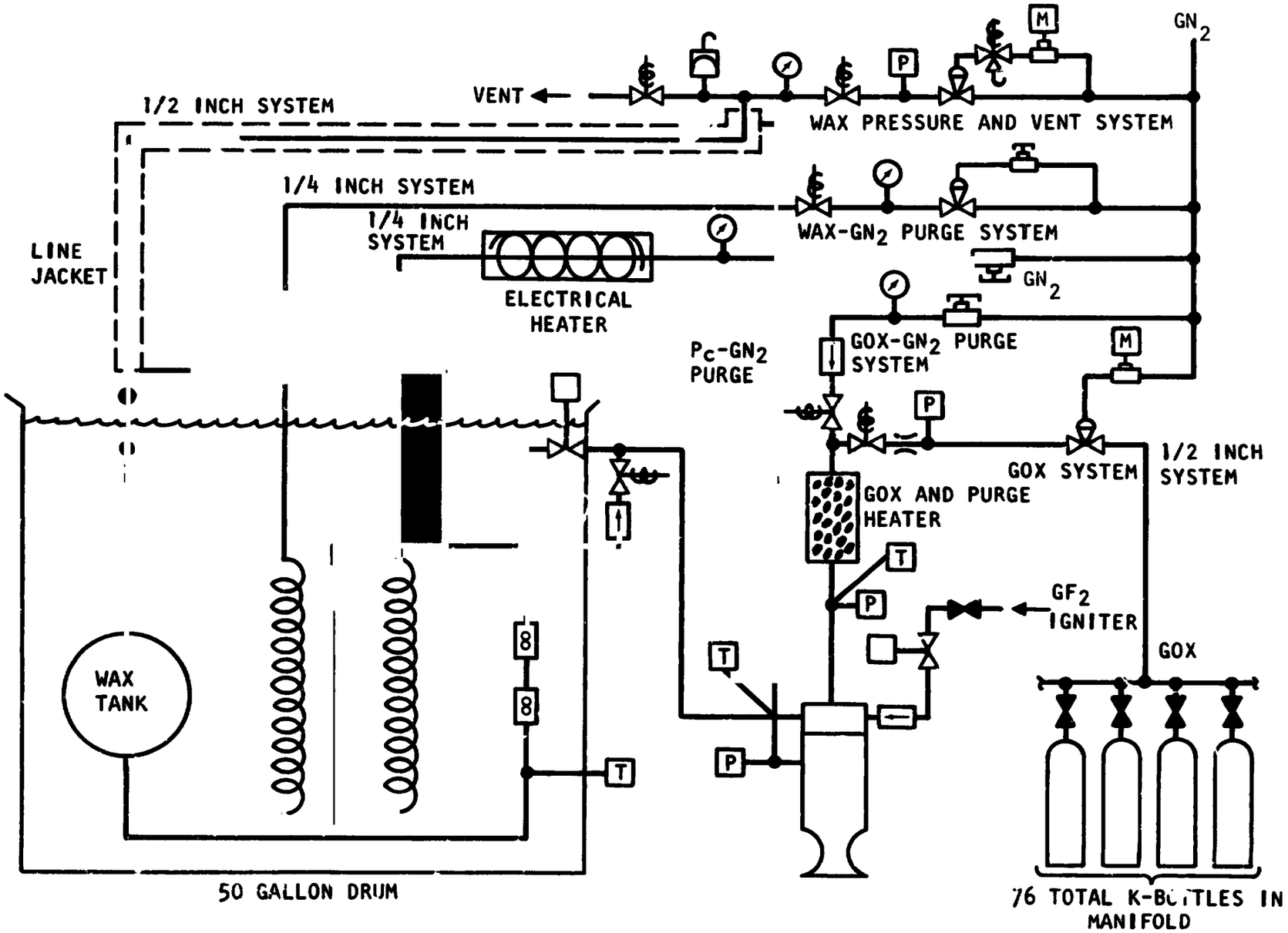

Figure 9. Schematic of Hot-Fire Facility

calculations, the chamber pressure measured just upstream of the chamber convergence section is used. It should be noted that the P_c purge is turned off after steady-state combustion is achieved so that the actual chamber pressure can be measured. All instruments were calibrated weekly.

All data were recorded on circular or strip chart graphic recorders for instant readout as well as on the high-speed Beckman Acquisition System. The data were then processed directly from the data tapes on the IBM 360 computers.

RESULTS

Hot-fire experiments were conducted to determine the combustion characteristics of the propellants over a wide range in contraction ratio and chamber length. These results are used to specify both the overall mixing and vaporization efficiency of the engine. Subsequently, analytical combustion models were run for the conditions specified for the hot-fire experiments to predict performance characteristics as a function of the initial spray dropsize. Comparison of the experimental and analytical performance characteristics are used to specify an "apparent" spray dropsize which is required to produce the hot-fire characteristics. This value of apparent dropsize is lastly compared with that predicted using dropsize correlations determined for wax in cold-flow experiments (Ref. 4). These results are discussed below.

EXPERIMENTAL TESTING

A total of 44 tests was conducted; however, only 18 tests yielded usable data. This was due to two problems that were encountered. Tests 1 through 22 were invalid because of unsteady fluctuating flowrates. Removal of the initial wax tank, which was composed of three parallel-plumbed, 3-inch-diameter tubes, and replacement with a single 2-gallon spherical tank remedied this problem. Tests 30, 43, and 44 resulted in subsonic nozzle throat flow due to low chamber pressure. Data from those tests were therefore not included in the final data analysis. The remainder of the data are presented in Table 6. Note that in addition to the basic measurements and the calculated measured c* efficiency, a chamber heat loss correction has also been included. The heat loss can be quite significant due to the large surface area of the chamber design.

For many of the tests, the resulting chamber pressures were low because of low c* performance. Due to tank pressure limitations, however, it was not possible to increase the wax flowrate in order to increase the chamber pressure to the desired value of 50 psia. This condition resulted in some tests in which the nozzle may not have been choked. For the low chamber pressure tests, verification that sonic flow occurred was accomplished in two ways: (1) calculation of

TABLE 6. SUMMARY OF HOT-FLOW DATA GOX/SHELL WAX 270

Test No.	L, inches	ε_c	L* inches	$P_{c(total)}$, psia	η_{c^*} meas	Q_T, Btu/sec	$\eta_{H.L.}$	η_{c^*} corr	MR
24	15	6	99	36.5	84.0	130	1.056	88.7	2.77
25	15	6	99	39.1	85.0	130	1.055	89.7	2.11
26	10.3	6	70.6	37.0	79.8	90	1.043	83.2	2.38
27	10.7	2	21.6	21.6	46.3	37	1.053	48.7	2.43
28	6	6	44.8	34.1	71.4	50	1.030	73.5	2.19
29	6	6	44.8	41.5	71.0	50	1.030	73.1	2.48
31	39	2	80	33.4	71.3	305	1.184	84.4	2.32
32	39	2	80	36.0	70.2	299	1.186	83.3	1.81
33	30	2	61	31.2	68.5	220	1.145	78.3	2.53
34	24	6	153	37.2	85.4	197	1.083	92.5	2.89
35	24	6	153	37.6	81.6	182	1.084	88.4	2.47
36	24	6	153	37.3	83.1	185	1.082	89.9	2.5
37	24	6	153	41.6	85.7	198	1.083	92.8	3.02
38	15	2	31	22.7	54.9	80	1.082	59.4	3.12
39	15	2	31	20.2	46.6	50	1.071	49.9	2.61
40	15	2	31	20.2	46.6	50	1.071	49.9	2.53
41	15	6	100	36.1	82.5	127	1.057	87.2	2.79
42	15	6	100	42.9	82.0	127	1.058	86.8	2.99

$$\eta_{H.L.} = 1 + \left(\frac{C^*_T}{C^*}\right)^2 \left(\frac{Q_T}{\dot{w}_T \, C_{p_g} \, T_c}\right)$$

the one-dimensional critical pressure ratio including the case where the chamber velocity is not zero and (2) review of the high-speed movies of the nozzle exhaust to observe whether or not shock patterns were present. The critical pressure ratio for nonzero initial velocity can easily be shown to be equal to:

$$\frac{P_1}{P_2} = \left\{1 + \frac{\gamma - 1}{2} \left[\frac{M_1^2 \left(1 + \frac{\gamma - 1}{2} (M_1^2)\right)}{1 + \left(\frac{\gamma - 1}{2}\right)}\right]\right\}^{\gamma/\gamma-1} \qquad (3)$$

where

P = static pressure

γ = specific heat ratio

M = Mach No.

1,2 = chamber and throat, respectively.

For $\varepsilon_c = 2$, $M_1 = 0.31$, and $\gamma = 1.2$, whereupon

$$\frac{P_1}{P_2} = 1.69$$

Therefore, for a contraction ratio of 2.0, the minimum static pressure in the chamber is (assuming $P_2 = 13.5$ psia)

$P_1 = 22.6$ psia ($P_{total} = 24$ psia)

at $\varepsilon_c = 2$

It should be noted, however, that when the nozzle has an expansion section, choked flow can be obtained at even lower chamber pressure than the one-dimensional calculations predict.

Inspection of Table 6 shows that Tests 27, 38, 39, and 40 have total pressures* less than this value. Inspection of the movies showed that Tests 27 and 38 appeared to be choked and 39 and 40 were not choked. Since the total pressures were reasonably close to the sonic condition, these tests were included in the data summary and subsequent analysis.

For all tests the inlet wax temperatures were about 205 F. The entire injector was preheated to at least 190 F to ensure that the wax would not freeze in the injection tubes. In addition, the gaseous oxygen was also heated to about 200 F.

Heat transfer from the combustion gases to the walls of an uncooled thrust chamber results in a loss of enthalpy and thus decreases the attainable chamber pressure. This energy loss is significant for the large chamber surface areas used in this program. Equation 4 was used for the determination of performance degradation due to chamber heat loss (Ref. 1).

$$\eta_{HL} = \left\{1 + \left[\frac{c^*_{theo}}{c^*_{meas}}\right]^2 \left[\frac{\sum(q/A)A}{\dot{w}_T \, c_{p_m} \, T_c}\right]\right\}^{1/2} \qquad (4)$$

where

c^*_{theo} = theoretical characteristic velocity at test conditions, based on full shifting equilibrium

c^*_{meas} = measured characteristic velocity, corrected for the previously discussed losses

$\sum(q/A)A$ = observed heat loss to chamber walls

$\dot{w}_T$ = total propellant flowrate

c_{p_m} = mean specific heat of combustion chamber gases at test conditions

T_c = theoretical combustion gas temperature at test conditions

---

*For the experimental data, the measured static pressure (near the beginning of convergence) was converted to the total pressure using standard one-dimensional pressure ratios. At ε_c of 2 and 6 the pressure ratios were $(P_{c\ static}/P_{total})$ 0.937 and 0.993, respectively.

Total heat loss to the chamber walls, in Btu/lb of propellant, was obtained by summation of calculated heat fluxes over the appropriate areas as discussed in Appendix A. It should be noted that the heat flux along the constant area portion of the chamber is not equal to the calculated theoretical value due to incomplete combustion. This effect is accounted for in Eq. 4 by reducing the theoretical adiabatic flame temperature of the combustion gases. In Eq. 4 this is $\left(\eta_{c^*theo}/\eta_{c^*meas}\right)^2$. These results in conjunction with Eq. 4 were used to determine $\eta_{H.L.}$ as shown in Table 6.

The data shown in Table 6 are plotted in Fig. 10a. The results are presented in terms of the corrected c* efficiency (corrected for heat loss) and mixture ratio. While it had originally been expected to present the data at a constant mixture ratio of 2.0, due to variable wax system pressure drops, the actual mixture ratios grouped more closely to 2.5 than 2.0. To minimize the extrapolation, the results are presented in Fig. 10b in terms of $(\eta_{c^*})_{corr}$ vs L* at a mixture ratio of 2.5. Note that when presented in terms of L* in Fig. 10b, the data fall on a single line regardless of contraction ratio. Since the droplet vaporization is approaching completion as the chamber length is increased, the maximum level of performance approaches the mixing-limited value, which appears to be about 90-percent c* efficiency. These results show that reasonably uniform mixing was achieved.

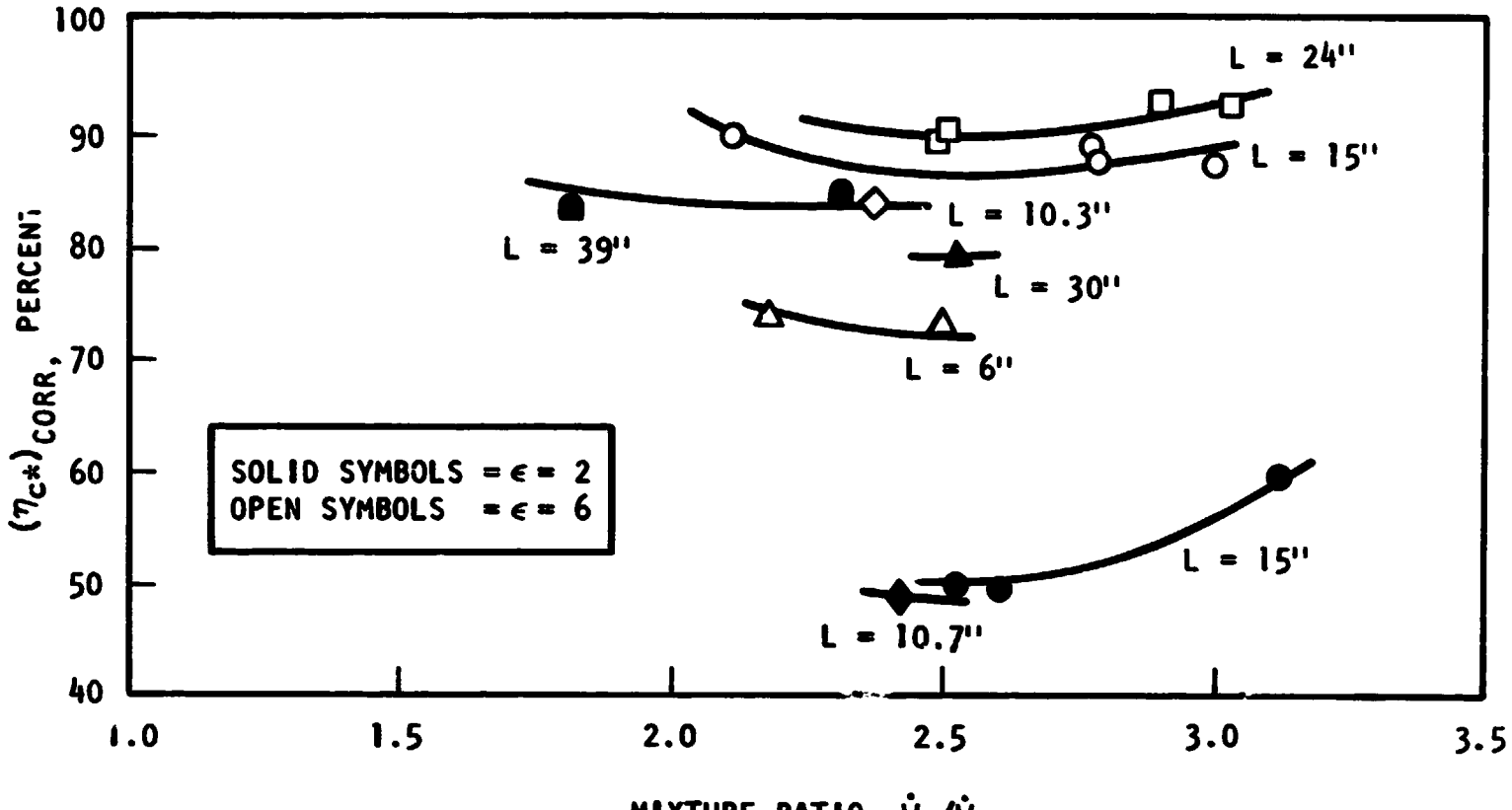

a. MIXTURE RATIO

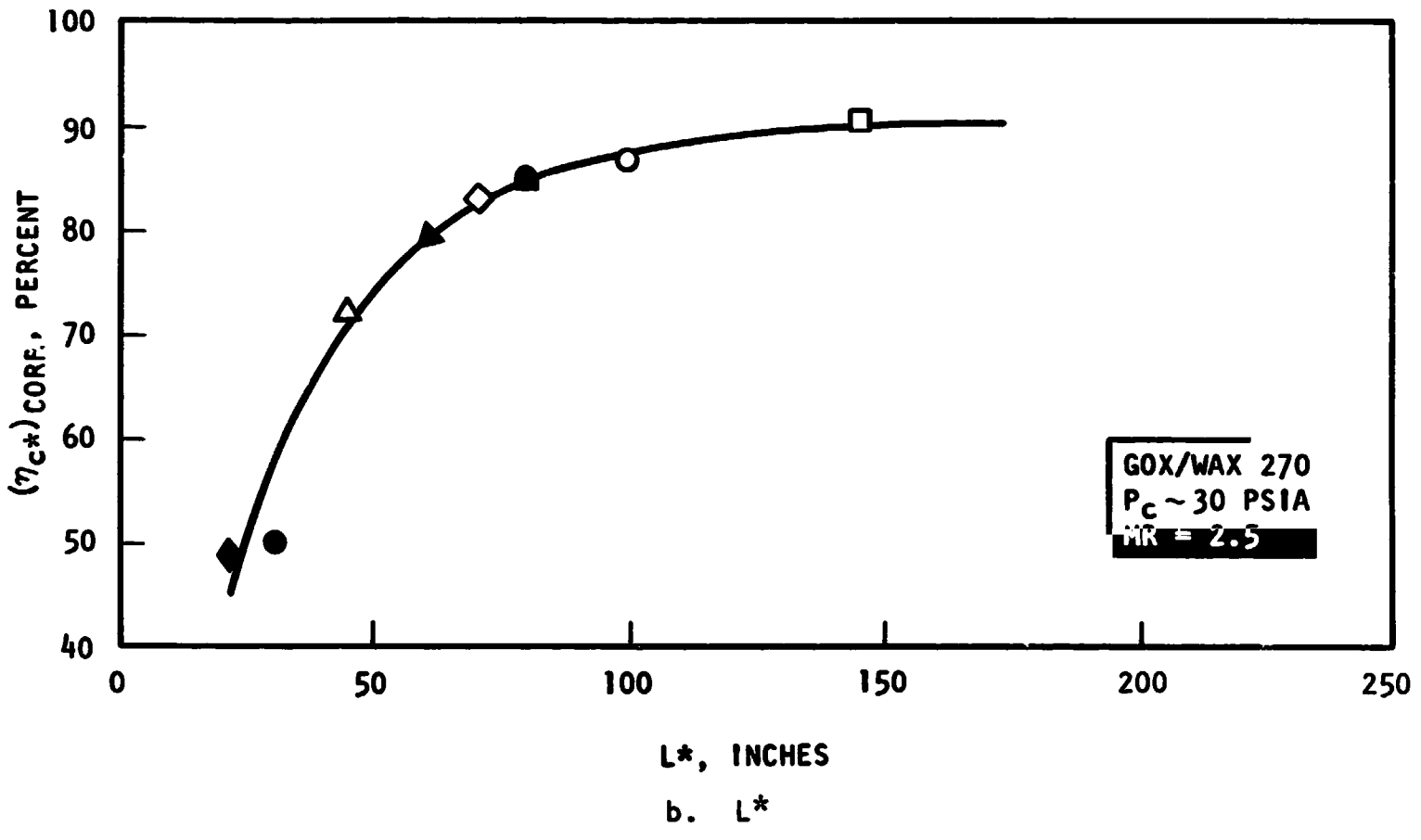

b. L*

Figure 10. Hot-Fire c* Performance Results as a Function of Mixture Ratio and L*

ANALYTICAL COMBUSTION MODEL RESULTS

An existing combustion model was used to calculate the predicted vaporization characteristics as a function of chamber geometry and initial dropsize. A complete description of the DER program is presented in Ref. 7. Since the sensible heat rise to bring the injected droplets to the boiling point is quite substantial for the Shell Wax 270 ($T_{initial}$ = 200 F) the droplet heating version of the DER model was employed (Ref. 8). In addition, the program was operated in two modes: (1) the single-stream tube and (2) multiple-stream tube analyses. In the first instance the mixing is assumed to be uniform, i.e., the existence of a nonuniform mixture ratio distribution does not affect the vaporization efficiency. Consequently, mixing losses are accounted for separately. In the second case, the mixture ratio was assumed to be nonuniform and the coupled effect of mixture ratio striations on vaporization efficiency was calculated directly by the model.

DESCRIPTION OF MODEL

The DER computer program requires data describing gas and spray mass and mixture ratio distributions and spray droplet sizes at a start plane for stream tube combustion calculations. These can either be specified or can be determined using the LISP (Liquid Injector Spray Pattern) section of the computer model. Using LISP, analysis begins with calculations of spray mass fluxes, velocity vectors, and droplet diameters at a large number of (r, θ) mesh points in a "collection plane" some short distance downstream of the injector face. These calculations are based on injector design data (number and type of injection elements, element locations, and orientation) and empirical parameters that correlate a single injection element's spray mass flux distribution and mean droplet size with its design and operating parameters. Approximations are also made of propellant vaporization (burning) that occurs upstream of the coll .on plane.

The output from LISP provides the necessary description of the two-phase flow field for initializing the stream-tube combustion program, STC. As mentioned above, the LISP computer model was used for multistream tube calculations; its collection plane becomes the STC initial plane.

Once the propellant flows are specified for an individual stream tube, the propellant flows (both sprays and gases) are constrained to flow in that tube, without exchanges of mass, momentum, or energy among neighboring stream tubes. Analytical model solutions are obtained numerically for several systems (one for each stream tube) of simultaneous ordinary differential and algebraic equations by starting with known conditions at the initial plane and marching downstream in small axial steps. Satisfaction of the throat boundary conditions depends upon the consistency of the initial data, particularly the initial plane pressure and flowrates, and the overall vaporization efficiency.

In the droplet heating version of the DER computer program, the temperature of droplets is transient. Once a droplet reaches its wet-bulb temperature, vaporization proceeds in a manner equivalent to that of the evaporation coefficient model. (The entire droplet is assumed to be at the wet-bulb temperature.)

Input to the above described model consists of chamber geometric wall profile, propellant properties, equilibrium combustion gas properties, and either (1) initial-plane gaseous flowrate and mixture ratio and spray flowrates, velocities, and droplet temperatures and diameters for all spray size groups entering each stream tube or (2) data from LISP from which these variables can be calculated. Up to 40 stream tubes can be initialized with as many as 12 spray size groups (fuel and oxidizer combined) in each. However, for this study only 10 stream tubes and 6 spray size groups were used.

SHELL WAX 270/GOX MODEL INPUT VALUES AND INITIAL CONDITIONS

The combustion model required a great deal of input data which are not readily available. Many physical properties of the Shell Wax 270 had to be estimated, equilibrium combustion performance of the wax/GOX propellants had to be calculated, and initial conditions for the start plane of the combustion model had to be determined.

Determination of Effective Molecular Structure of Shell Wax 270

Shell Wax 270 is a distillation cut mixture of petroleum hydrocarbons. According to the supplier, it contains predominantly straight-chain, paraffinic hydrocarbons, C_nH_{2n+2}, with a mean chain length of $30 \leq n \leq 35$. Wax physical and thermochemical properties were estimated, as discussed later, by assuming a single particular value of $n = 35$. This was determined to be the most suitable value in the following way.

Spray droplet heating and vaporization (burning) rates are functions of a number of variables, viz.: droplet diameter; initial droplet temperature; gas stream temperature; gas properties; droplet species properties, including liquid density, vapor pressure, and heat of vaporization, liquid and vapor specific heats, vapor thermal conductivity and viscosity, vapor diffusivity in the gas stream, and vapor state properties; and the relative convective velocity between a droplet and its surroundings. Uncertainties in any of these variables lead to uncertainties in burning rates calculated by a spray combustion model. Concerning species properties, the calculated burning rate usually is most sensitive to the heat of vaporization, vapor specific heat, vapor diffusivity and thermal conductivity of the vapor-gas film surrounding a droplet.

During the period of this contract, Allison at Pennsylvania State University conducted a number of single droplet burning experiments with Shell Wax 270 (Ref. 9). Wax droplets were suspended in low velocity combustion gas streams produced by an atmospheric pressure burner. The gas stream temperature and compositions were varied to simulate, approximately, various air/wax equivalence ratios. Motion pictures taken during the droplets' lifetimes provided data concerning droplet warm-up to equilibrium vaporization conditions and droplet vaporization or burning rates. Quasi-steady vaporization rate data were given for a number of droplets; those for one droplet are shown as the experimental data in Fig. 11.

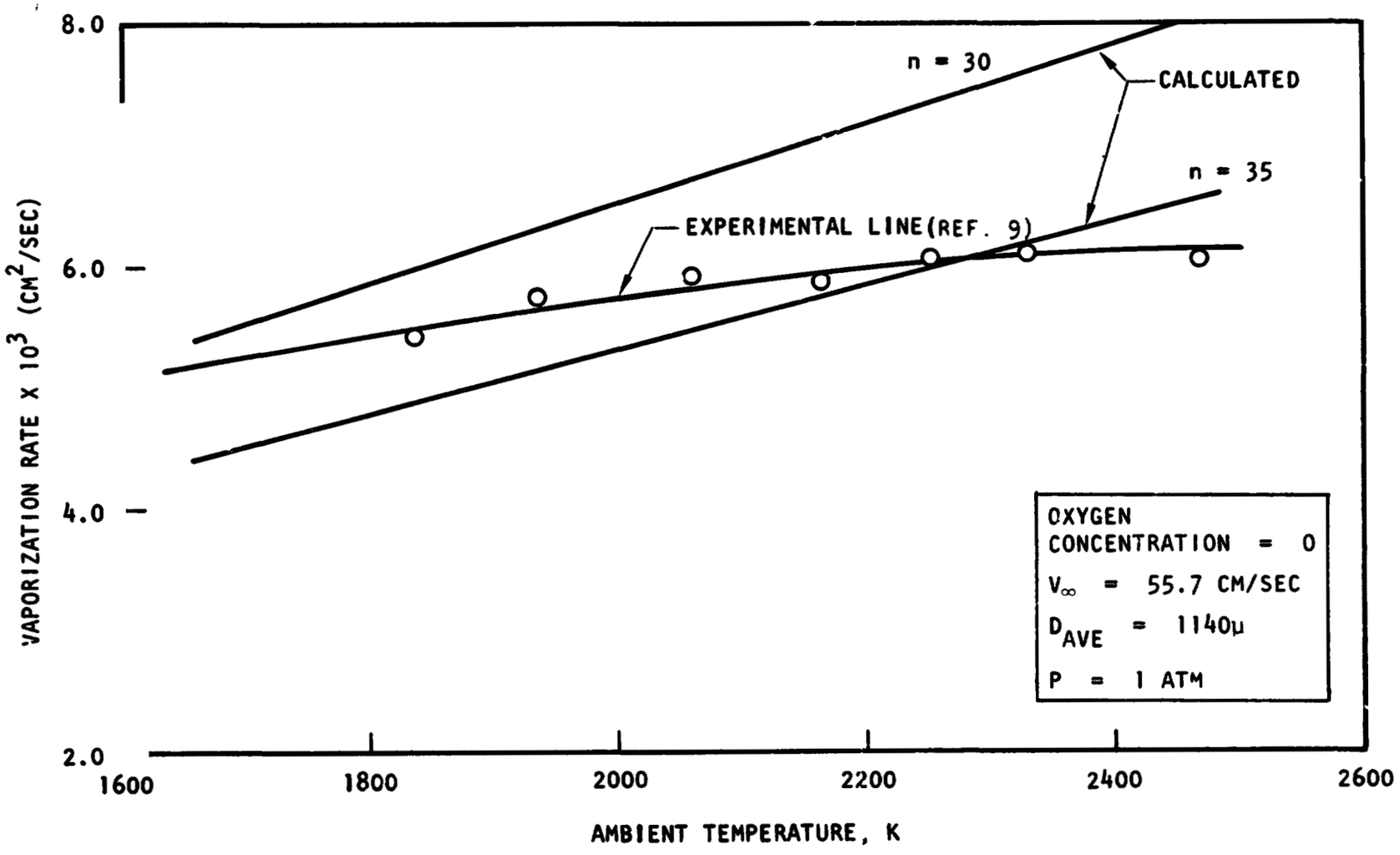

Figure 11. Vaporization Rate vs Temperature for Shell Wax 270

Allison's data were used to provide an empirical adjustment of the Shell Wax 270 properties provided to the spray combustion model. This was done by performing model calculations for some of his experimental conditions and varying, initially, the paraffin chain length, n. (For each n, wax properties were estimated as described below.) Calculated burning rates for n = 30 and for n = 35 are plotted in Fig. 11, along with Allison's experimental data. Although the calculated variation of burning rate with gas stream temperature was somewhat greater than was observed, the n = 35 curve was in generally good agreement with the experimental data. Sensitivity to wax properties was checked by arbitrarily varying the assumed values of heat of vaporization and vapor specific heat by about 50 percent. Only very modest displacements and changes in slope of the calculated burning rate curves of Fig. 11 resulted. Therefore, a value of n = 35 was assumed, with wax properties estimated as follows.

Physical Properties Used in Model

The physical properties of $C_{35}H_{72}$ are not directly available. However, physical properties of shorter length hydrocarbon chains are available, and they are generally "smooth" functions of the number of carbon atoms, n.

Known values of critical pressure and temperature and the heat of vaporization and liquid density at the normal boiling point were plotted (Fig. 12) as functions of n, and curves were drawn through them and extended up through n = 35 to estimate the required values.

The mole fraction of wax vapor at the liquid surface as a function of both pressure and temperature was estimated as follows:

$$X_v(P,T) = \frac{P_v(T)}{P} \quad (5)$$

with

$$\ell n \frac{P_v}{P_{crit}} = \xi [T_d - T_{crit}] \quad (6)$$

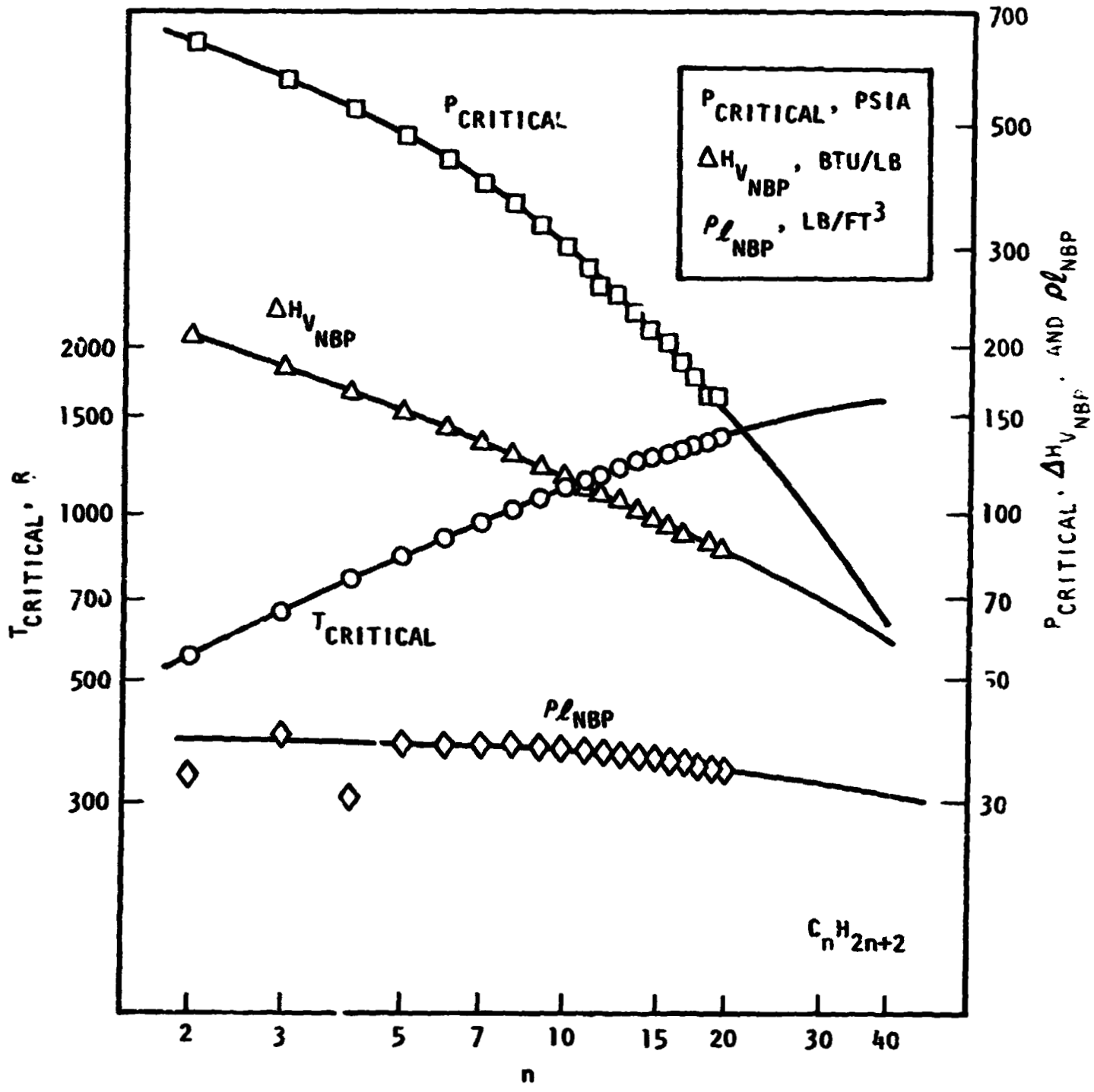

Figure 12. The Effect of Hydrocarbon Chain Length on Several Physical Properties

and

$$\xi = \frac{\ell n \left[\frac{P_v\ (T_{NBP})}{P_{crit}} \right]}{T_{NBP} - T_{crit}} \tag{7}$$

where

P = pressure
T = temperature
X = mole fraction
d = droplet
NBP = normal boiling point
v = vaporization

Heat of vaporization was considered to vary with droplet (liquid) temperature by the relation:

$$\Delta H_v(T_d) = \Delta H_v(T_{NBP}) \left[\frac{T_{crit} - T_d}{T_{crit} - T_{NBP}} \right]^{0.38} \tag{8}$$

where

ΔH_v = heat of vaporization (effective)

The model uses the Redlich-Kwong equation of state to determine the pressure. This equation is

$$P = \frac{RT}{[v - b] - \left[a/[\sqrt{T}\ \ v(v + b)] \right]} \tag{9}$$

where

R = gas constant
v = specific volume

The "a" and "b" coefficients for the equation of state were also calculated from Eq. 9 based on properties at the critical and normal boiling point.

A time-share computer program was used to estimate viscosity of the wax vapor as a function of temperature. The Chapman-Enskog equation using Lennard-Jones potential parameters (tabulated in Ref. 10) and based on known values of critical pressure and critical temperature, is the method coded in this program.

A special time-share computer program was written to help calculate the required binary diffusion coefficient parameters. A fundamental equation given in Ref. 10 was used to calculate binary diffusion coefficients for wax/O_2, wax/wax, wax/CO_2 and wax/H_2C systems each over a range of temperatures. The latter two systems were appropriately combined for the wax/combustion product coefficients and all of the values were then reduced to the parameter required for input to the combustion model.

Finally, the combustion gas properties, e.g., stagnation temperature, molecular weight, specific heat, viscosity, and characteristic velocity, c*, were obtained as functions of mixture ratio and stagnation pressure using the Rocketdyne "n-element"equilibrium computer program. The theoretical shifting c* performance is shown in Fig. 1.

Dropsize Distribution

The dropsize distribution input into the model taken from Ref. 4 is presented in Fig. 13. This distribution was obtained using Shell Wax 270 in a like-doublet configuration and therefore should match that produced by the injector designed in this study. Note that the largest dropsize obtained was about 2.4 times the mass median size.

Specification of Initial Percent Vaporized

The combustion analysis model requires spray and gas flowrates to be specified at an axial plane where the stepwise calculations through the chamber are initialized. The percentage of the spray vaporized between where it was formed and the initial plane was determined in a manner to be compatible with the initial plane location and the initial burning rate. The combustion model was

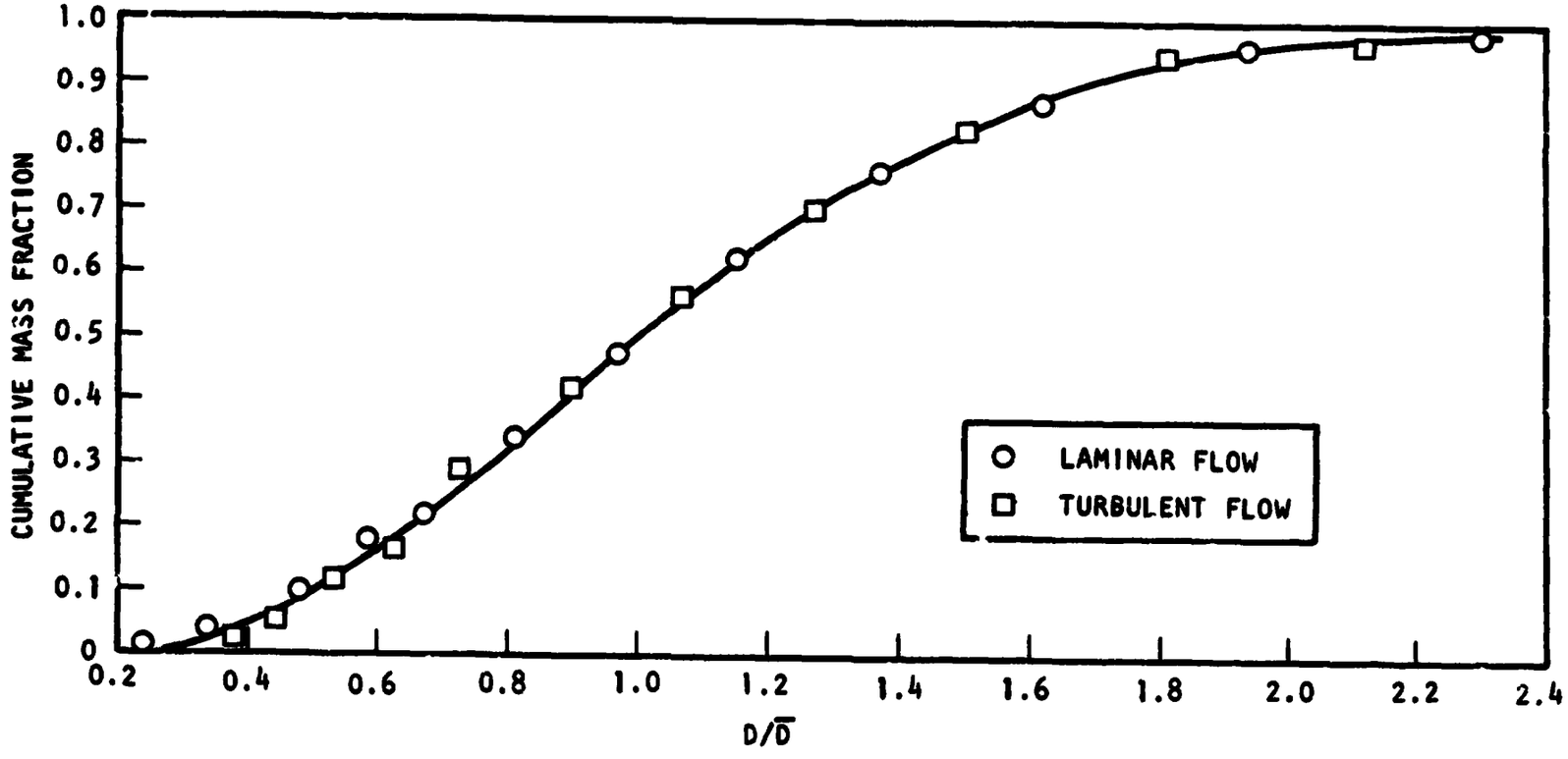

Figure 13. Comparison of Dropsize Distributions Produced by Laminar and Turbulent Jets

run first with just a rough estimate of 5 percent wax spray vaporized at 1/2 inch from the injector face, and the percentage burned versus the axial location calculated from the combustion model was determined. The results are shown in Fig. 14. These results suggested that the initial percent vaporized of 5 percent is too large since extrapolation of the percent vaporized to the injector face results in a discontinuity. Smaller initial percentages of fuel vaporized were also assumed and the resulting characteristics determined. A value of 1-1/2 percent fuel initially vaporized was finally chosen since it resulted in a "reasonably" continuous curve when extrapolated to the injector face (see the lower curve on Fig. 14).

Determination of Mass and Mixture Ratio Distribution

For the multistream tube analysis, mass and mixture ratio distribution of the spray at the initial plane were required. This could not be satisfactorily accomplished with the LISP section of the DER computer model because of its restriction to chambers with circular cross sections. Instead, the LISP equations were specially programmed for a single like-doublet element forming spray in a rectangular chamber. The spray distribution shape coefficients were analyzed separately and provided as input to the special computer program. The spray distribution and corresponding η_{c^*} were solved at incremental distances. The distance at which η_{c^*mix} matched the experimental efficiency was determined, and this mass distribution was used for determining the spray mass going into discrete stream tube area segments in the initial plane for the multiple stream tube combustion analysis. The mass was specified for the stream tubes by summing the computed mass as a function of mixture ratio and then dividing the mass into ten equal mixture ratio segments.

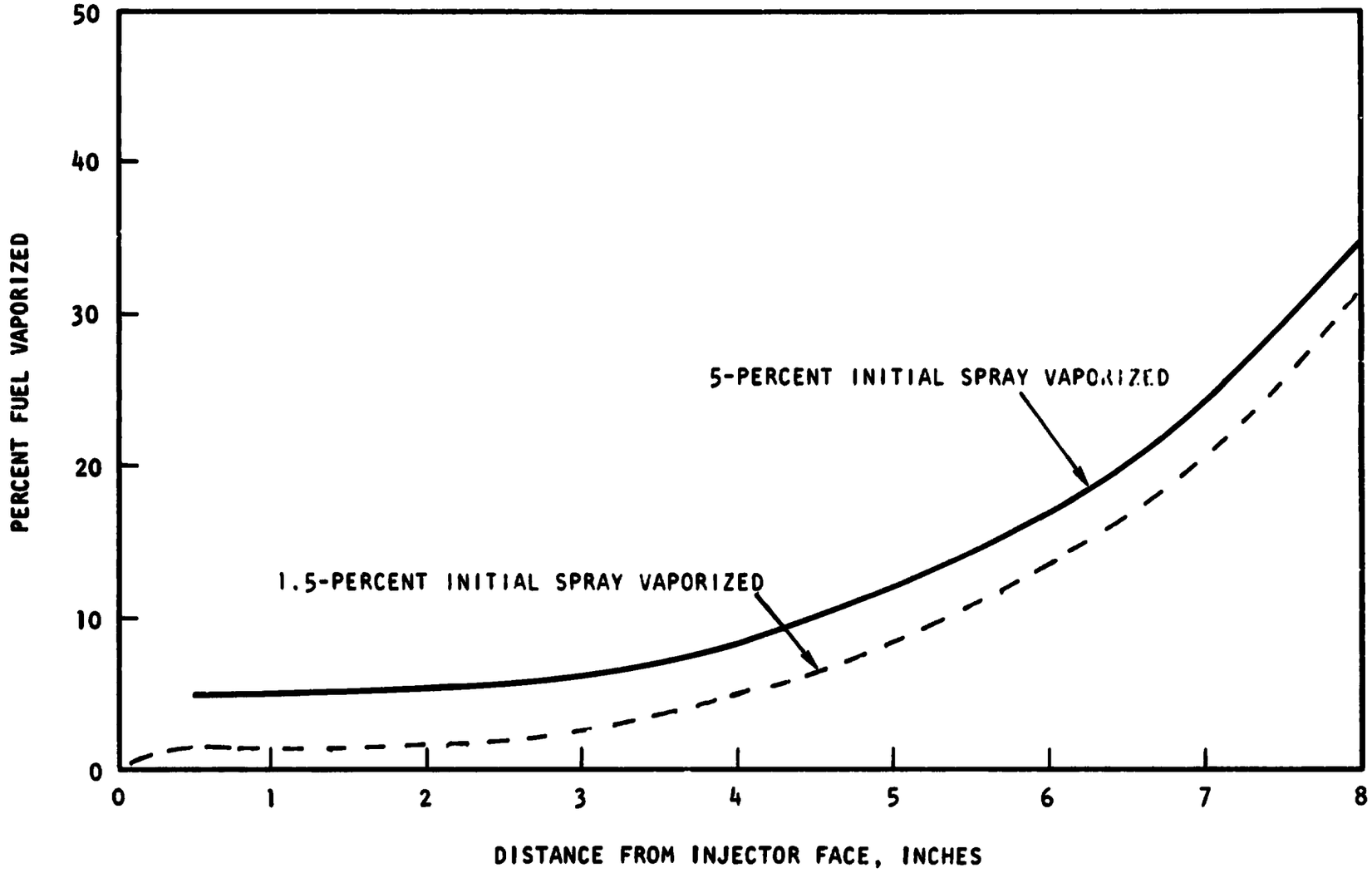

Figure 14. The Resulting Percentage Vaporization as a Function of Chamber Length as Predicted From the DER (Droplet Heating) Computer Model

SHELL WAX 270/GOX PERFORMANCE PREDICTIONS

Single-Stream Tube Model Analysis

Single-stream tube model calculations were accomplished to define the vaporization limited c* performance characteristics (η_{vap}) over a range of characteristic length (~15 to 80 inch l*) contraction ratio (2 and 6) and mass median dropsize (100 to 300 μ). The operating conditions were:

GOX/Shell Wax 270	MR = 2.5
P_c = 35 psia	Propellant Injection Temperature = 200 F

The results for the two contraction ratio configurations are presented in Fig. 15 and 16, respectively. Comparison of the results shows a surprisingly large difference between the level of performance attained (at equal L* and $\bar{D}$ conditions) for each contraction ratio. Since L* is related to the droplet stay time in the combustion chamber, it was originally assumed that the performance predictions for these contraction ratio engines would be nearly equal. (Note for a 300μ mass median dropsize, the η_{vap} performance is about 30 percent higher for the ε of 2 than that for the ε of 6.) Subsequent calculations showed that this large performance difference was due to the droplets requiring a proportionately longer fraction of their chamber residence time to reach their boiling temperature for ε_c = 6 than for ε_c = 2.

Two additional calculations were conducted with the propellant injection temperatures equal to the wax boiling temperature. The results of these calculations are listed in Table 7.

TABLE 7. COMPARISON OF PERFORMANCE AT TWO DIFFERING INITIAL PROPELLANT TEMPERATURES

T_{wax}, F	L*, inches	$\bar{D}$, microns	ε_c	η_{vap}, percent	$\Delta\eta_{vap}$, percent
200	78.5	300	2	89.5	29
200	78.5	300	6	60.5	
1380	78.5	300	2	99.9	3.4
1380	78.5	300	6	96.5	

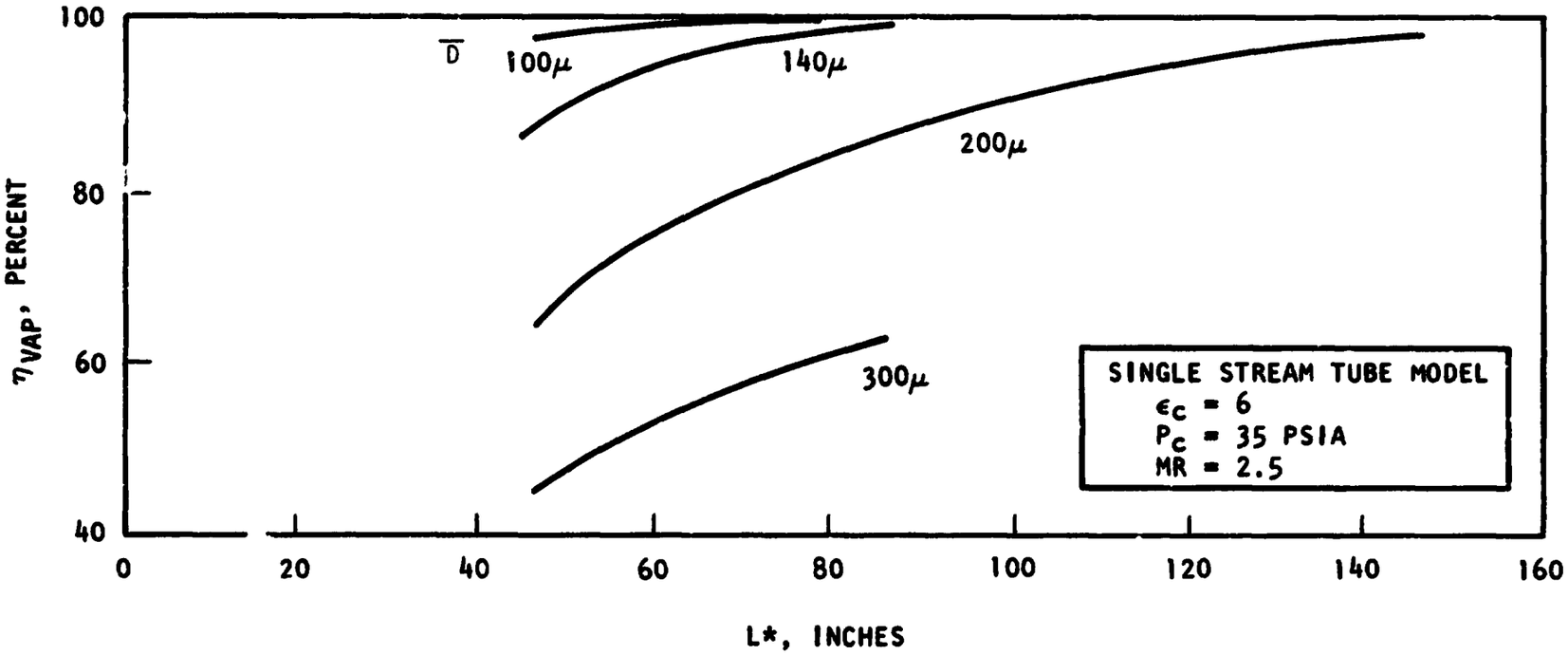

Figure 15. Single Stream Tube DER (With Droplet Heating) Combustion Model c* Performance Predictions, ε = 6

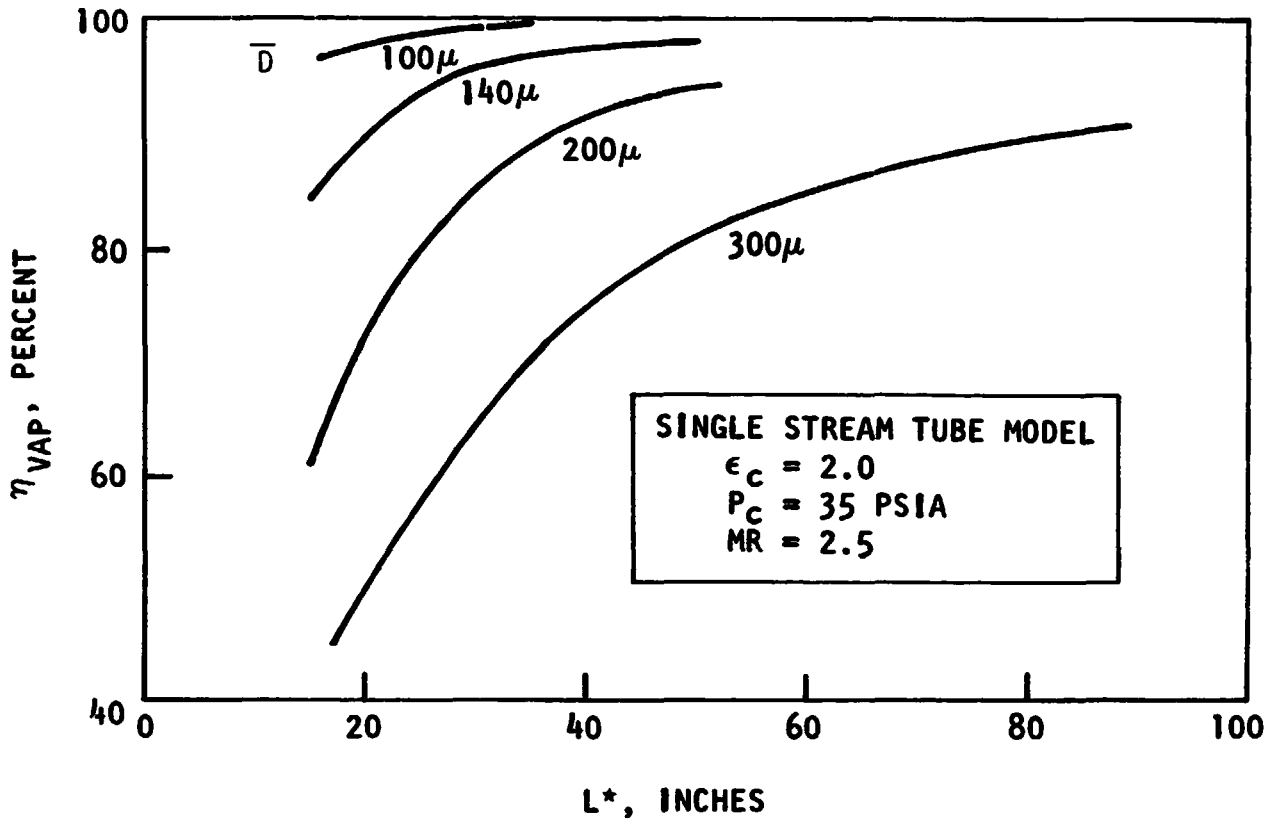

Figure 16. Single Stream Tube DER (With Droplet Heating) Combustion Model c* Performance Predictions, ε = 2

As shown, the difference in η_{vap} for zero heat-up time to droplet boiling, between the contraction ratio 2 and 6 configurations, is only 3.4 percent. This difference is similar to those normally obtained with the K-Prime or conventional DER model.

Based on the calculated results shown in Fig. 15 and 16, 100 percent η_{vap} can only be obtained for initial mass median dropsizes on the order of 200 μ or smaller. However, even for these values of mass median dropsize excessive chamber L*'s are required. It is obvious from these plots that injecting the wax into the combustion zone at a temperature of 200 F leads to the necessity of using large chamber lengths to achieve complete vaporization.

Multistream Tube Model Analysis

To assess the influence of nonuniformity of mixture ratio on vaporization, the propellants were assumed to be distributed in the manner discussed above to produce an overall η_{mix} of 90 percent and several multistream tube runs of DER were made. The value of η_{mix} = 90 percent was obtained from the hot-firing data (Fig.10b). For the contraction ratio of 6 configuration, the results of the multistream tube calculations are presented in Fig. 17. Comparison of the single and multistream tube, Fig. 15 and 17, results at 200 μ shows that a difference of 5 percent in η_{vap} occurs at an L* of 80 inches. As illustrated in Fig. 17, this performance difference between the results leads to an appreciable difference in the dropsize predicted at a given η_{vap} and L*. It is felt from these results that determination of the apparent dropsize, by comparison of actual and predicted performances, should be accomplished using the multistream tube results.

One multistream tube calculation was made for the contraction ratio of 2 engine configuration. The result compared with that obtained using the single stream tube analysis is presented below.

ε = 2.0	Single Stream Tube Analysis	η_{vap} = 83 percent
L* = 28 inches	Multistream Tube Analysis	η_{vap} = 87 percent
$\bar{D}$ = 200 μ		

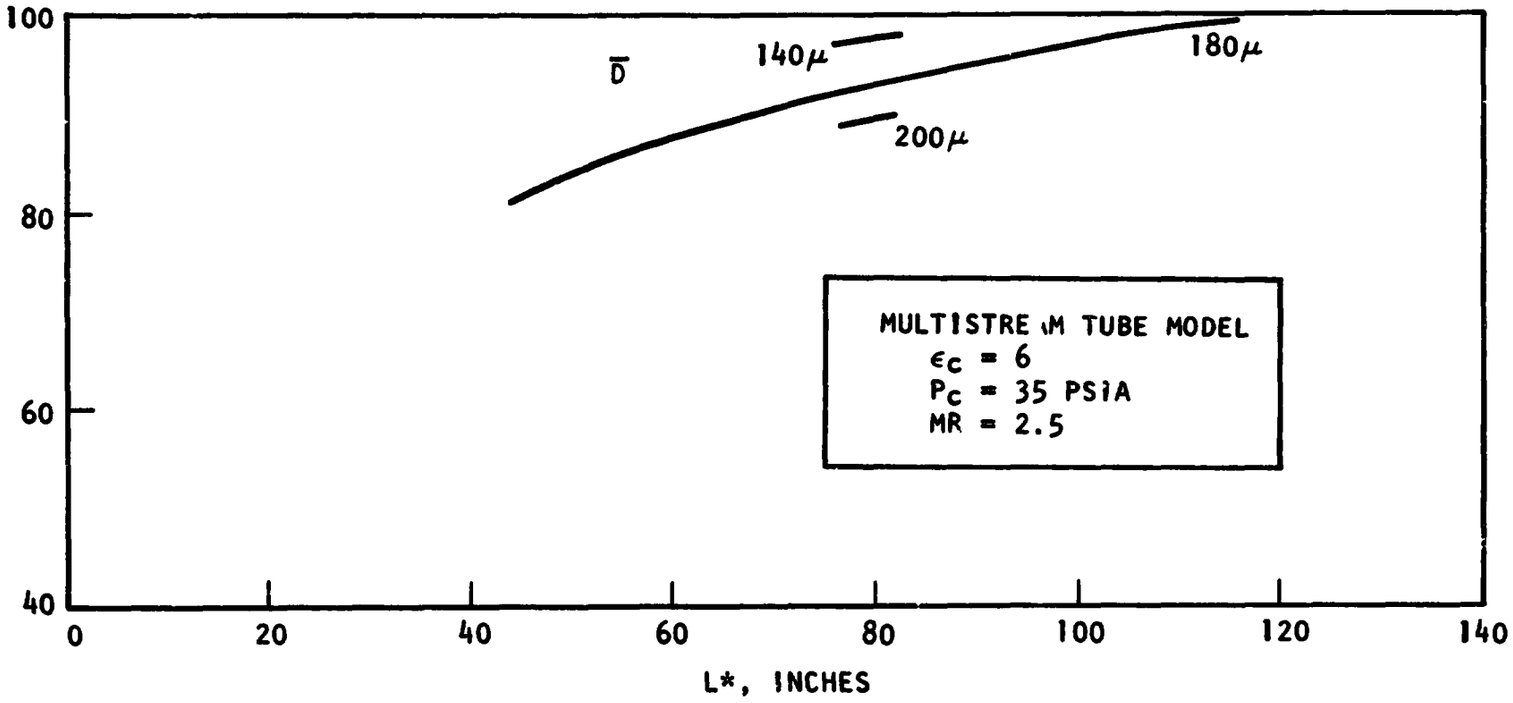

Figure 17. Multistream Tube DER (With Droplet Heating) Computer Model c* Performance Predictions, ϵ = 6

This result is similar to that found for the contraction ratio of 6. The difference in η_{vap} for this configuration is 4 percent.

Combustion Gas Velocity as a Function of Chamber Length

In addition to η_{vap} characteristics the combustion model also determines the axial gas velocity as a function of the chamber length. The average gas velocity from the multistream tube analysis is shown plotted as a function of chamber length in Fig. 18 at the contraction ratios of 2 and 6, for the initial wax temperature of 200 F, and initial dropsize of 225 microns. The initial gas velocities are shown at an axial distance of 0.5 inch. This location is 0.171 inch downstream of the impingement point (located at X = 0.329 inch) and was used as the initial start plane for the stream tube analysis. Since the gaseous oxygen is injected at relatively high velocity at the injector face and quickly diffuses to a relatively low velocity (~20 at ε = 6, and 60 at ε = 2) just upstream of the impingement point it is difficult to extrapolate the gas velocity to the injector face with any certainty. For subsequent purposes, however, only the value of gas velocity near the impingement point is required so that no attempt was made to estimate the gas profile at smaller chamber lengths.

It is of some interest to compare the gas velocity profiles as predicted assuming the wax droplet heat-up time to be negligible with those discussed above. The gas velocity profiles obtained for the wax injected near the boiling temperature are also shown in Fig. 18. The gas velocity profiles are significantly different at both contraction ratios. Note that the gas velocity levels attained are considerably higher for zero heat-up time as compared with the 200 F wax temperature results. Since the chamber cross-sectional dimensions were set assuming that the higher gas velocity at ε = 2 would turn the sprays, these results suggest that the chamber width at a contraction ratio of 2 may be too small and that substantial amounts of wax spray may impinge on the wall. (This is discussed in detail later.)

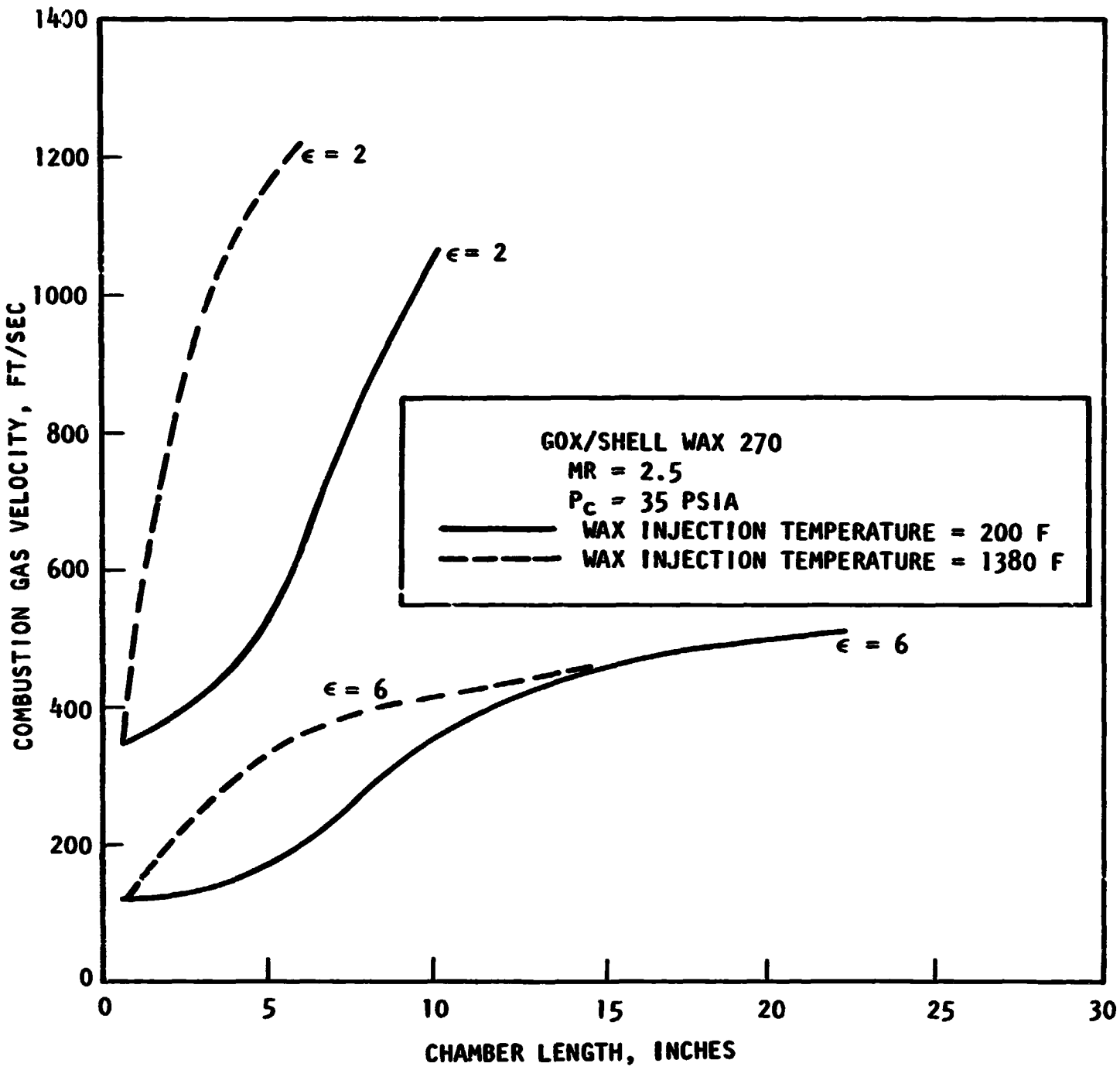

Figure 18. DER Combustion Model Predictions of Velocity as a Function of Chamber Length

DISCUSSION OF RESULTS

COMPARISON OF EXPERIMENTAL C* PERFORMANCE WITH COMBUSTION MODEL PREDICTIONS

SINGLE STREAM TUBE MODEL COMPARISONS

The c* performance measured in the experimental tests included the loss due to incomplete mixing and incomplete vaporization. The mixing-limited c* performance was determined experimentally by increasing the chamber length sufficiently until complete vaporization occurred. As the chamber length increases, the measured c* efficiency will asymptote to the value corresponding to the mixing limited performance, η_{mix}. The η_{vap} is then simply determined by (Ref. 1):

$$\eta_{vap} = \eta_{c^* \text{ corr}}/\eta_{mix} \qquad (10)$$

The hot fire performance values shown in Fig. 10 must first be corrected for the mixing loss before superimposing them on the combustion model predictions for $\eta_{c^* \text{ vap}}$. Inspection of Fig. 10 shows that the mixing-limited performance for the contraction ratio of 6 data is 90 percent ($\eta_{c^* \text{ corr}}$). Since the contraction ratio of 2 data seems to merge with the ε of 6 data and in addition yields identical performances in the range of L* where they overlap, it can be assumed that the mixing-limited performance for both chamber configurations is 90 percent.

The experimentally determined vaporization c* efficiencies are compared to the single stream tube combustion model predictions in Fig. 19 and 20. Note that a constant apparent dropsize is predicted when the data are compared in this manner for either contraction ratio configuration. However considerable differences in the apparent dropsizes for each contraction ratio are predicted. Average values of the apparent dropsize are 300 and 160 microns for the contraction ratios of 2 and 6 respectively. Contrary to that initially expected, this result shows that the overall apparent dropsize for the small contraction ratio (2) configuration is larger than for the large contraction ratio (6). In addition, the results suggest that the dropsize, although different at each condition, was nevertheless constant as a function of chamber length and consequently secondary breakup did not occur.

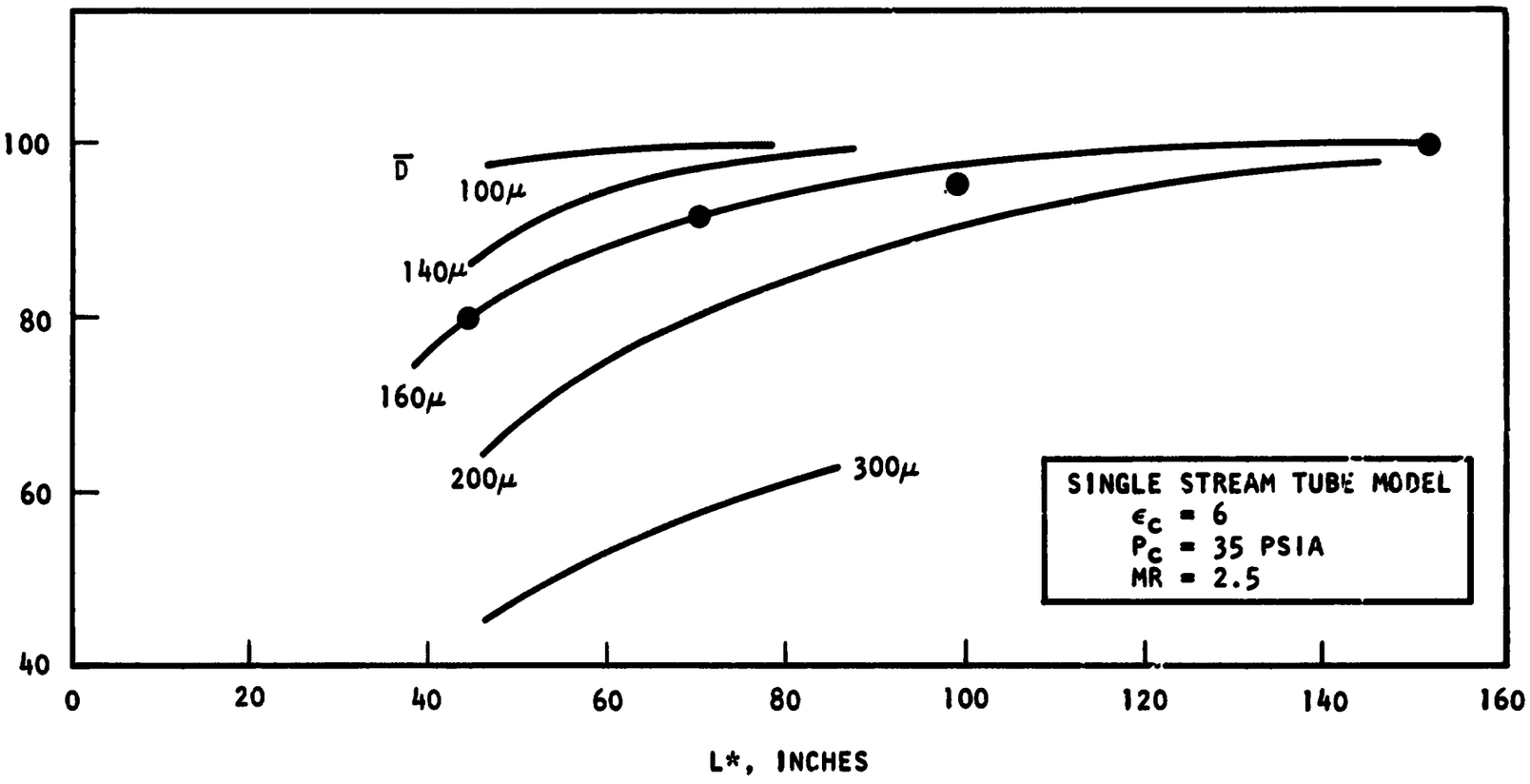

Figure 19. Single Stream Tube DER (With Droplet Heating) Computer Model c* Predictions Compared With Hot-Fire Results, ε = 6

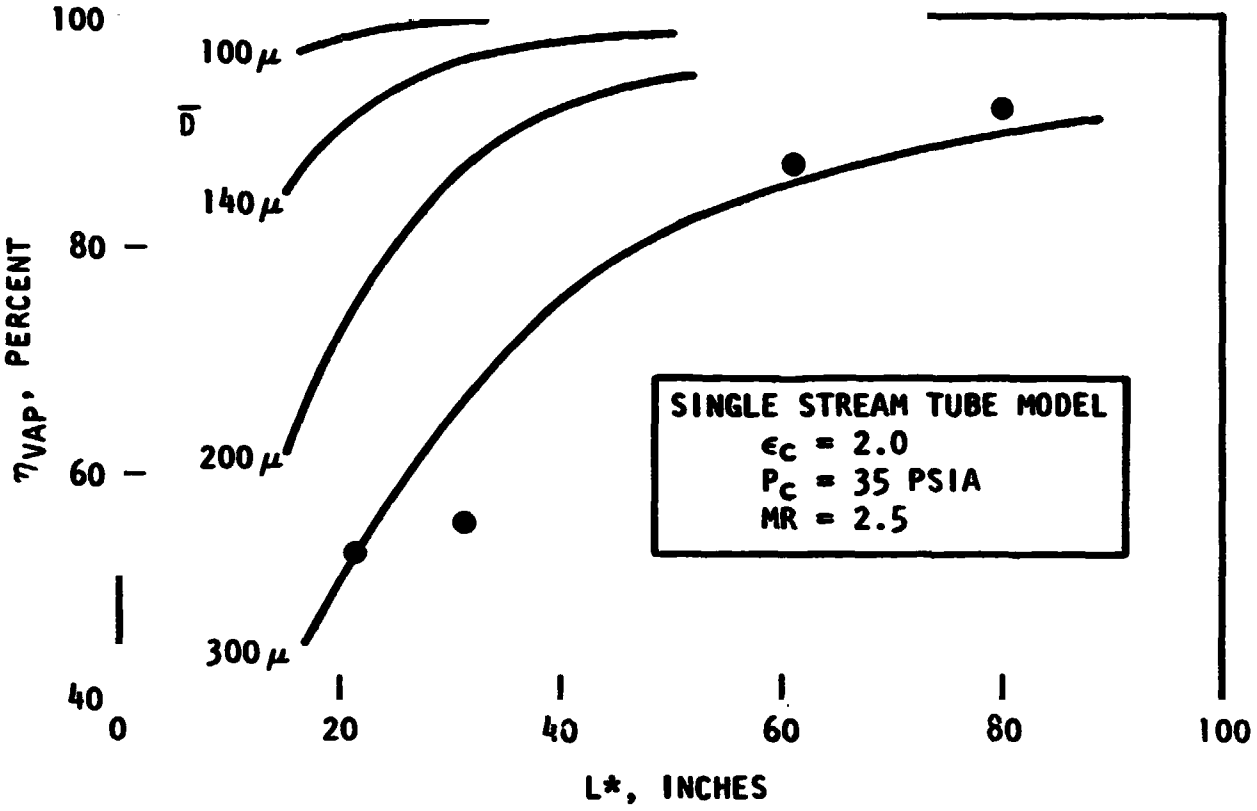

Figure 20. Single Stream Tube DER (With Droplet Heating) Computer Model c* Predictions Compared With Hot-Fire Results, ε = 2

The importance of using combustion models to interpret experimental results is vividly illustrated by these results. As shown previously the experimental results alone showed that the performance characteristics for both engine configurations were similar. In addition, since L* is proportional to the stay time of droplets within the combustion zone, the experimental results would suggest that the same initial and final droplet sizes were produced at both contraction ratios. This interpretation would be substantially correct for normal propellants not requiring large droplet heating times to initiate vaporization. (The closeness of the c* performances at the heated wax condition for equal dropsizes and L* was discussed in the previous section.) However, for the gaseous oxygen/ Shell Wax 270 propellant combination the combustion model analysis reveals that in order to obtain the experimentally determined performance characteristics the dropsize at a contraction ratio of 2 must have been considerably larger than that occurring at ε of 6.

This interpretation is considerably different than that which would have originally been concluded without the aid of the combustion model, since the injector used and the quantities of propellants injected were identical in both contraction ratio engines. Therefore, due to gas velocity differences the apparent dropsize for the ε of 2 configuration was expected to be less than that obtained at a contraction ratio of 6.

Interpretation of these results requires first the determination of the apparent dropsizes using the multistream tube combustion model predictions and comparison with the initial dropsize predicted from the empirical correlations of Zajac (Ref. 8 and 4).

MULTISTREAM TUBE MODEL COMPARISONS

The apparent dropsize determined in the same manner as for the single-stream tube case, is presented in Fig. 21 for the 6 to 1 contraction ratio data. The solid line shown on the figure is the performance characteristics predicted from the combustion model for a 180μ mass median diameter spray. The comparison of the

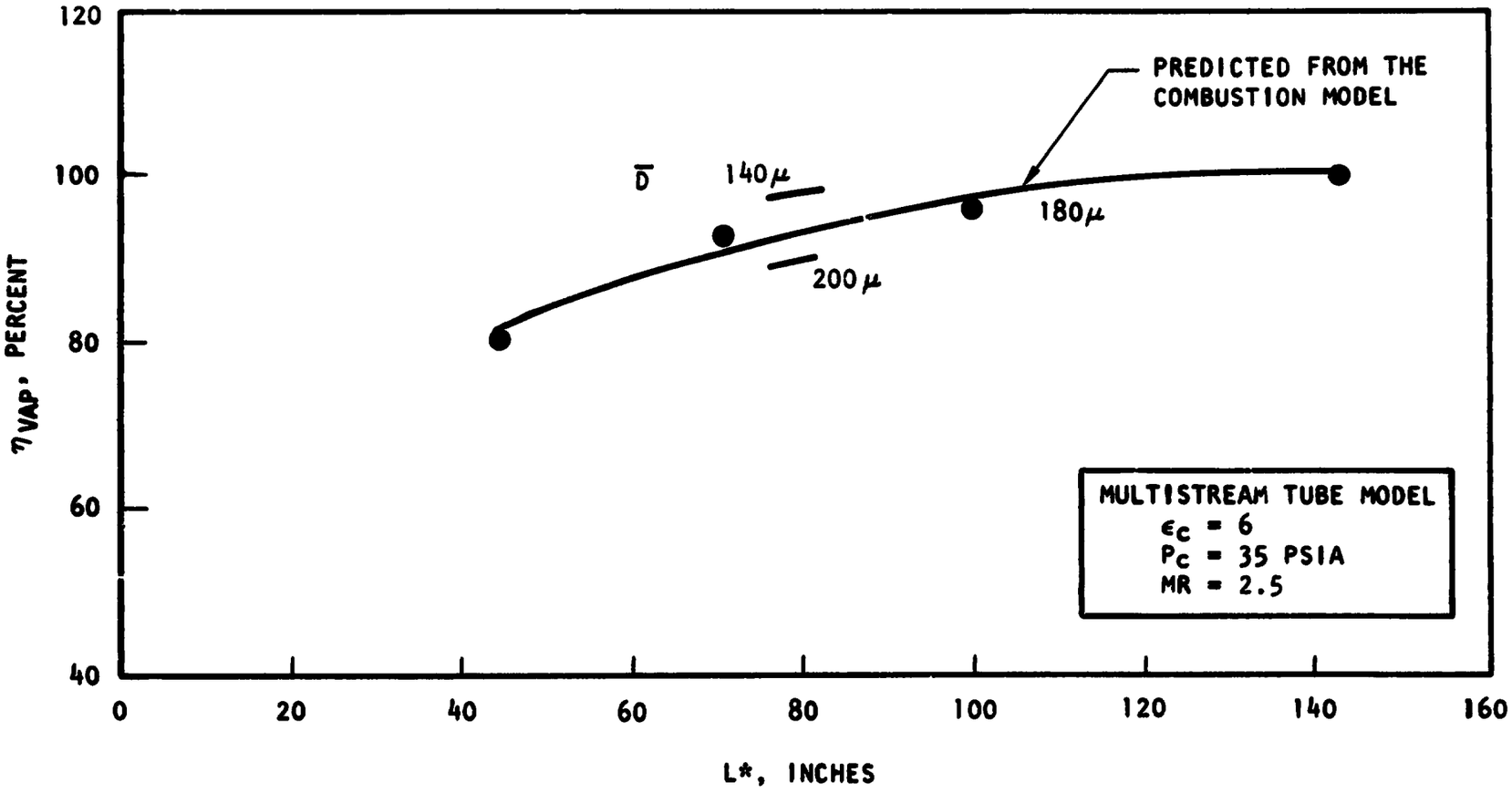

Figure 21. Multistream Tube DER (With Droplet Heating) Computer Model c* Predictions Compared With Hot-Fire Results, ε = 6

experimental data with this prediction shows excellent agreement over the entire range in L*. This model appears to correctly predict both the trends and level in performance with variations in chamber length. A similar analysis for the contraction ratio of 2 was not conducted due to funding limitations. However, the results of the single-point multistream tube calculations presented under the Results section suggests that the same differential in dropsize between single- and multistream tube analyses as shown from the contraction ratio of 6 results should also apply for the contraction ratio of 2 configuration. Consequently, the apparent dropsize predicted for a contraction ratio 2 would be about 320 microns.

COMPARISON OF APPARENT DROPSIZE WITH COLD-FLOW PREDICTED DROPSIZE

CONTRACTION RATIO 6 CONDITIONS

A meaningful comparison of the apparent dropsize determined in the manner described above with cold-flow predicted dropsize is dependent on two factors: (1) the ability to determine the initial input dropsize assuming zero combustion gas velocity and (2) the determination of the effect of gas velocity on dropsize. The determination of the initial (V_g = 0) dropsize can be determined from existing empirical correlations (Ref. 4). The effect of gas velocity on the atomization process using Shell Wax 270, under noncombustion conditions to date, has only been determined over limited ranges. Fortunately, the range of experiments is within that of this study so that an estimate of the gas velocity effect on atomization can be made.

The dropsize produced as a result of two wax jets impinging in a quiescent atmosphere has been extensively studied by Zajac (Ref. 4). The orifice size, L/d_j and injection velocity for these experiments are within the range for which Eq. 11 (Ref. 4) was developed.

$$\overline{D} = k\, V_j^{-1.0}\, (P_c/P_j)^{-0.10}\, d_j^{0.57} \qquad (11)$$

where

- k = 15.9 x 10^4 for Shell 270 Wax (T_{inj} = 200 F)
- V_j = mean injection velocity, ft/sec
- $\overline{D}$ = mass medium dropsize, microns
- d_j = orifice diameter, inches
- P_c/P_j = velocity profile parameter defined as the ratio of the centerline dynamic pressure to the mean dynamic pressure (Ref. 4)

Equation 11 can be used to calculate the dropsize produced by a like-impinging doublet element in a quiescent atmosphere. For the conditions of this study (as shown earlier in the Design section), the mass median dropsize is:

$$\overline{D} = 225\mu \text{ at } V_g = 0$$

Combustion processes occurring in the rocket engine can alter the initial dropsizes produced from the element, since the combustion gases near the impingement point and droplet formation zone are not zero. The magnitude and acceleration of the gases are influenced by the rate of vaporization, chamber contraction ratio, and droplet heat-up rate from 200 F to the boiling temperature. As shown previously, appreciable gas velocity levels exist even for the contraction ratio of 6 configuration. A study is currently being conducted (under NASA Contract NAS3-14371) to evaluate ranges of conditions which include those which were encountered in this study. Selected data from Contract NAS3-14371 are reproduced in this report to illustrate the effect of gas velocity on wax dropsizes over an applicable range of flow conditions applicable to the present combustion study (noncombustion). Preliminary data are presented in Fig. 22 showing the effect of gas velocity on dropsize for a constant-area chamber. (The gas velocity in the chamber is therefore essentially constant.) For these data the initial dropsize was about 200μ and injection velocity range from 180 to 200 ft/sec. Note that for a gas velocity of 200 ft/sec the mass median dropsize can be reduced by as much as 25 percent (200 to 150μ).

From these data, it is felt that dropsize is some function of gas velocity and the apparent dropsize can be determined accurately only by including the breakup characteristics as a function of length and breakup time in the combustion model. While droplet breakup requires some distance for completion, the results of Zajac suggest that burning droplets may therefore undergo secondary breakup as combustion proceeds The experimental results compared to the combustion model back calculations of the present study show that the dropsize were constant regardless of engine length. Thus, if secondary breakup occurred in the engine experiments, it probably occurred in the initial region of combustion where little vaporization

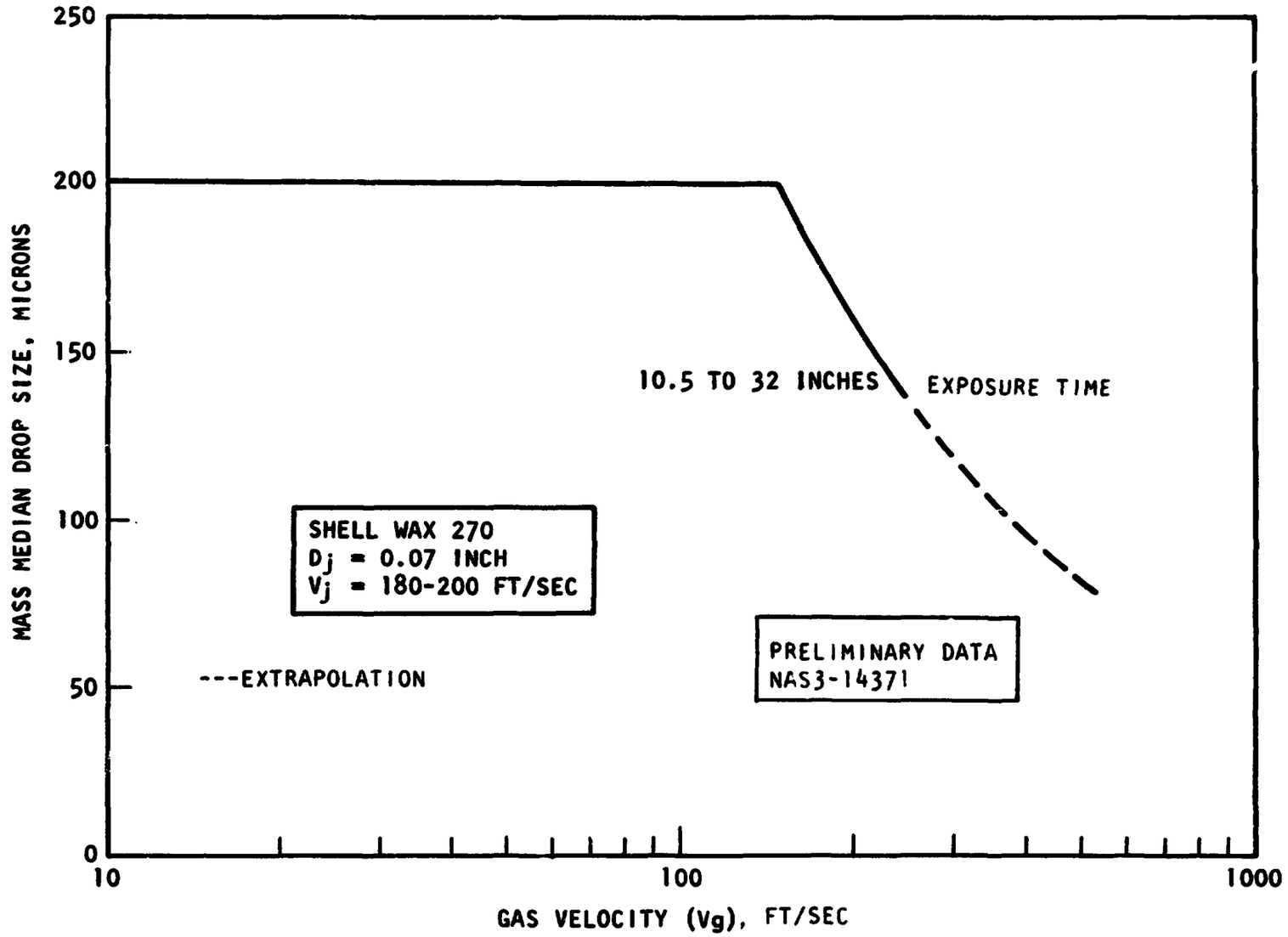

Figure 22. The Influence of Gas Velocity on the Dropsize Produced From a Like Impinging Doublet Injector (Cold Flow) in a Constant Area Chamber

had taken place. Consequently, the effects on the combustion model calculations would be to simply indicate a constant apparent dropsize with chamber length. The data from Fig. 22 suggest that for an average gas velocity in the first few inches of chamber length of 200 ft/sec (see velocity estimate for contraction ratio of 6 in Fig. 18) and a 225μ initial droplet, the dropsize obtained in a quiescent atmosphere could be reduced by as much as

$$\left[\frac{\overline{D}_{input}}{\overline{D}_{final}}\right]_{\text{Fig. 22 actual case}} = \left[\frac{\overline{D}_{input}}{\overline{D}_{final}}\right] \tag{12}$$

$$\frac{200\mu}{160} = \frac{225\mu}{\overline{D}_{final}}$$

$$\overline{D}_{final} = 179\mu$$

for

$$V_g = 200 \text{ ft/sec}$$

$$\varepsilon_c = 6$$

This value is essentially equal to that determined from the comparison of the experimental data with the analytical results shown in Fig. 21. It is not anticipated that this close agreement will always exist due to the approximations made in the combustion model, the assumptions required in the comparison, and the cursory method of extrapolating the data of Fig. 22. However, the comparison suggests that for this engine configuration the combustion model does adequately describe the droplet heatup and vaporization process. Furthermore, the experimental technique appears to be ideal for that determination.

CONTRACTION RATIO 2 CONDITIONS

For a contraction ratio of 2, the approach to the determination of the cold-flow dropsize is identical to that described for ε of 6. Since the flowrates through the injector were identical for both configurations, the initial dropsizes assuming zero gas velocity are equal (i.e., 225μ). The average gas velocity in the

initial region is about 700 ft/sec for a contraction ratio of 2; see Fig. 18. Based on the preliminary results of Lajac (Fig. 22), the final cold-flow predicted dropsize is

$$\frac{200}{75} = \frac{225}{\overline{D}_{final}}$$

$$\overline{D}_{final} = 84\mu$$

for

$$V_g = 700 \text{ ft/sec}$$

$$\varepsilon_c = 2$$

As stated earlier, the apparent dropsize predicted from comparison of the experimental data and combustion model back calculations resulted in a dropsize of 320μ. The large discrepancy between these values and the fact that the apparent dropsize at a contraction ratio of 2 is larger than that predicted at 6 suggests that for the contraction ratio of 2 other effects altered the initial dropsize produced via the injection scheme. The most likely possibility is that wall impingement of significant amounts of fuel occurred. This hypothesis is analytically substantiated below.

Because of the above suggestion, an estimate of the likelihood of spray impinging and accumulating on the wall was undertaken. The analysis consisted of writing the steady-state equation of motion in nondimensional form and solving it in two dimensions by finite difference techniques to define droplet trajectories. The solution was then obtained for several droplet size trajectories and the chamber dimensions were superimposed on the trajectories to determine the axial location where wall impingement would occur.

The problem to be solved is sketched below.

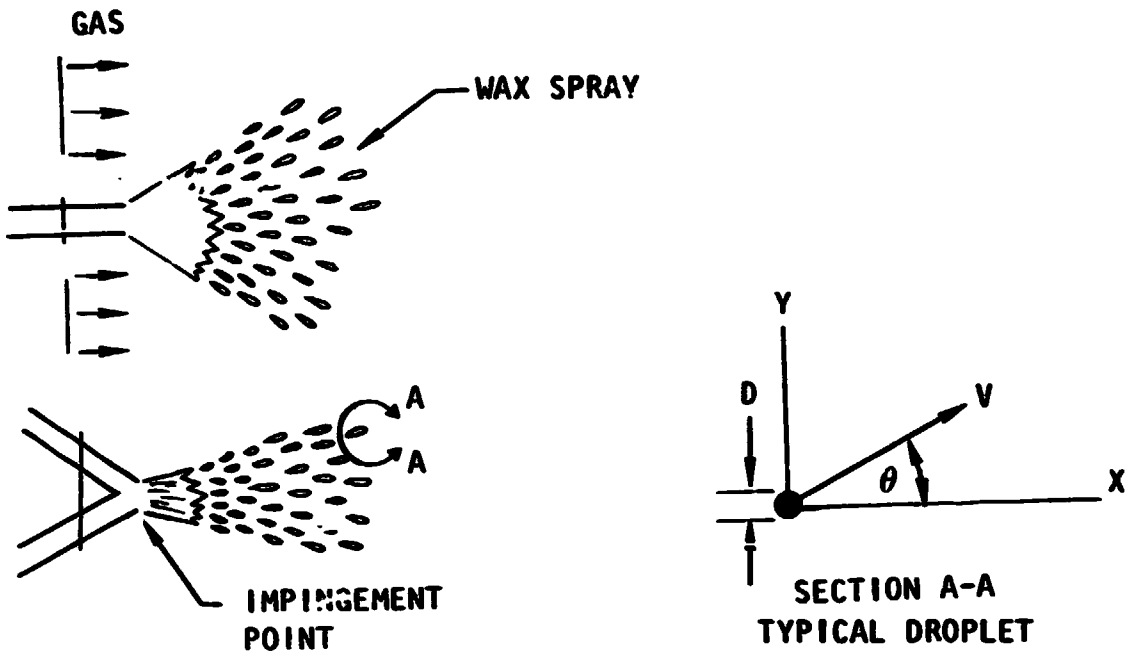

Figure 23. Sketch of Impingement Pattern

For the droplet the total derivatives of the x and y momentum are:

x - momentum

$$1/2\ \rho_G\ |\vec{u} - \vec{v}|\ (u_x - v_x)\ C_D\ \frac{\pi D^2}{4}\ -\ \frac{\pi D^3}{6}\ \frac{\partial P}{\partial x}\ =\ \frac{\pi D^3}{6}\ \rho_L \left(\frac{Dv_x}{D\ t}\right) \qquad (13)$$

y - momentum

$$1/2\ \rho_G\ |\vec{u} - \vec{v}|\ (u_y - v_y)\ C_D\ \frac{\pi D^2}{4}\ -\ \frac{\pi D^3}{6}\ \frac{\partial P}{\partial y}\ =\ \frac{\pi D^3}{6}\ \rho_L \left(\frac{Dv_y}{D\ t}\right) \qquad (14)$$

Assume

$$\frac{\partial P}{\partial x}\ =\ \frac{\partial P}{\partial y}\ =\ 0 \qquad (15)$$

$$u_y\ =\ 0 \quad |\vec{u}|\ =\ u_x$$

$$\rho_L\ =\ \text{constant}$$

$$\rho_g\ =\ \text{constant}$$

in Lagrangian terms, Eq. 13, 14, and 15 convert to

$$\frac{dV_x}{dt} = \frac{3}{4} \frac{\rho_G}{\rho_L} \frac{C_D}{D} |u_x - \vec{v}| (u_x - v_x) \tag{16}$$

$$\frac{dv_y}{dt} = \frac{3}{4} \frac{\rho_G}{\rho_L} \frac{C_D}{D} |u_x - \vec{v}| (-v_y) \tag{17}$$

$$dy/dx = v_y/u_x \tag{18}$$

if $$C_D = C_{D_o} \left(\frac{|u_x - \vec{v}| \rho_G D}{\mu} \right)^n$$

and if the variables are nondimensionalized in the following manner

$$\text{velocity}' = \text{velocity}/V_\infty$$
$$x' = x/L$$
$$y' = y/L$$
$$t' = t V_\infty/L$$
$$D' = D/L$$

where V_∞ = theoretical gas velocity at the beginning of convergence

L = chamber half width

Then Eq. 16, 17, and 18 are written as

$$\frac{dv_x'}{dt'} \left[3/4 \frac{\rho_G}{\rho_L} \frac{L}{D} C_{D_o} \left(\frac{V_\infty \rho_G D}{\mu_G} \right)^n \right] |u_x' - \vec{v}'|^{1+n} (u_x' - v_x') \tag{19}$$

$$\frac{dv_y'}{dt'} = \left[3/4 \frac{\rho_G}{\rho_L} \frac{L}{D} C_{D_o} \left(\frac{V_\infty \rho_G D}{\mu_G} \right)^n \right] |u_x' - v'|^{1+n} (-v_y') \tag{20}$$

$$\frac{dy'}{dx'} = \frac{V_y'}{u_x'} \tag{21}$$

Finally defining $\lambda \equiv 3/4 \frac{\rho_G}{\rho_L} \frac{L}{D} C_{D_o} \left(\frac{V_\infty \rho_G D}{\mu_G}\right)^n$ (22)

the final equations are

$$\frac{dv'_x}{dt'} = \lambda |u_x' - \vec{v}'|^{1+n} (u'_x - v'_x) \quad (23)$$

$$\frac{dv'_y}{dt'} = \lambda |u'_x - \vec{v}'|^{1+n} (- v'_y) \quad (24)$$

$$\frac{dy'}{dx'} = \frac{v'_y}{u'_x} \quad (25)$$

These equations were solved in finite difference form to determine typical droplet trajectories. The gas velocities used in the solution were those determined from the combustion model analysis and previously presented in Fig. 18. Typical values of the pertinent parameters used are listed in Table 8.

TABLE 8. SUMMARY OF CHARACTERISTIC DIMENSIONS AND PHYSICAL PROPERTIES

ε	$\bar{\mu}_G$, lbm/ft-sec	$\bar{\rho}_G$, lbm/ft^3	V_∞, ft/sec	L, inch	N_{Re}	ρ_G/ρ_L
2	6.2×10^{-5}	0.0124	1220	0.575	1825	0.00026
6	6.2×10^{-5}	0.0124	370	1.725	552	0.00026

The trajectory is, of course, dependent on the initial angle of the spray. Based upon numerous observations of similar sprays, a reasonable spreading angle for the narrow side of the spray is about 15 degrees half angle. For all subsequent calculations the initial angle of the spray was assumed to be 15 degrees. It should be pointed out that the droplet initial angles range from 0 to about 15 degrees (half angle). In addition, most of the mass is concentrated along the central portion of the spray. This is most easily seen by inspection of plots of mass contours for a like-impinging doublet shown in Fig. 24. Note that the highest mass flux levels are in the central position of the fan and that the mass flux drops dramatically to zero at the edges.

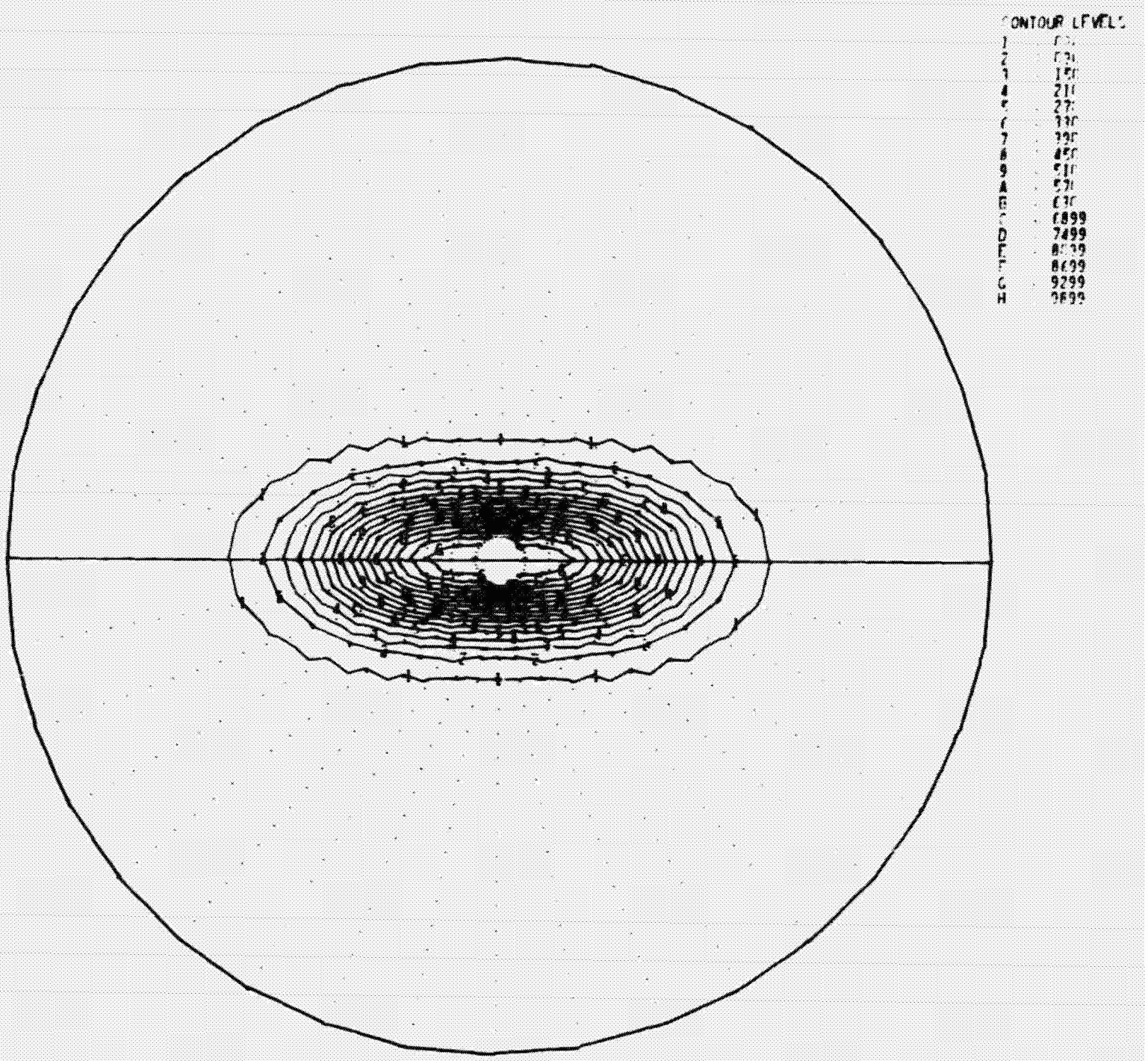

Figure 24. Fuel Flux Contour Plot

The determination of the drag coefficient was based upon the equations employed in the DER model. In particular, for the range in Reynolds number listed in Table 7, the drag equation is:

$$C_D = 0.271\ N_{Re}^{0.217} \tag{26}$$

To further simplify the calculations, for a Reynolds number of about 550 (ε_c=6) the C_D was assumed constant and equal to 1.0, while for a N_{Re} of 1800 (ε_c=2) the assumed C_D was 2.0. This simplification is certainly justified since C_D does not vary greatly with N_{Re} over this range. In addition, the solution for droplet trajectory is not sensitive to "small" variations in C_D.

Droplet trajectories for several sizes are given in Fig. 25a and b. A maximum dropsize of 564 was selected based on ~2.5 x $\bar{D}$ being the largest dropsize as indicated by the droplet distribution curve shown in Fig. 13. Note that for the contraction ratio of 6 configuration, the droplets will strike the wall in about 7 inches of chamber length, regardless of size. For the contraction ratio of 2, the larger droplet sizes will strike the wall at about 2.5 inches from the injector face and 100μ droplets will reach the chamber wall within 3-1/2 inches. It is surprising that even for the higher gas velocities encountered in the contraction ratio of 2 engine, these values are still insufficient to appreciably turn the spray. Consequently, in all probability at a contraction ratio of 2 a considerable quantity of mass will hit the chamber wall.

In addition to the above analysis, calculations were made of droplet trajectories for the case wherein the wax is injected into the combustion chamber near its boiling point. The gas velocity profile for a contraction ratio of 2 was shown in Fig. 18. The results of the analysis are shown in Fig. 26. Note that for this case, only the largest droplet sizes would reach the wall at about 3.5 inches downstream of the injector face. Consequently, if the wax were preheated the quantity of wax impinging on the wall would diminish.

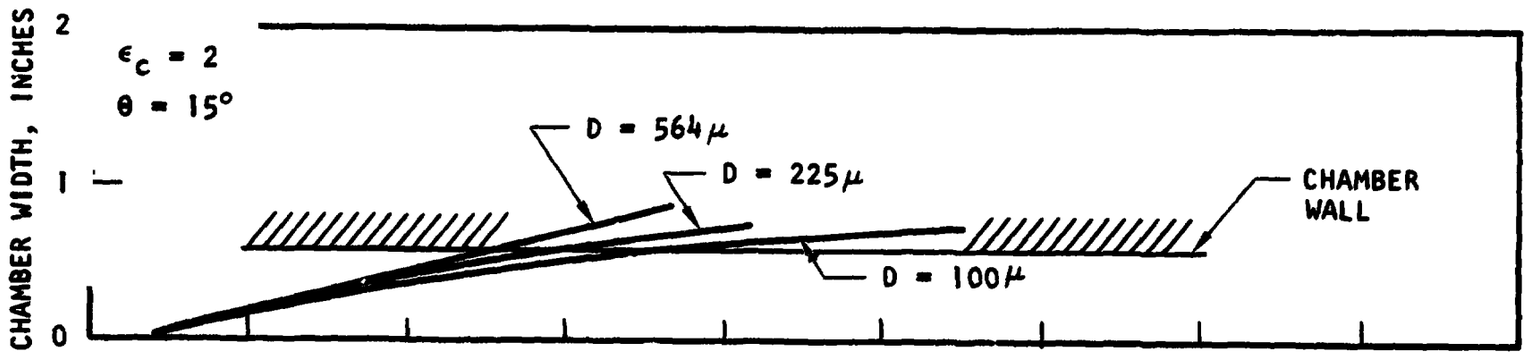

a. ϵ_c = 2

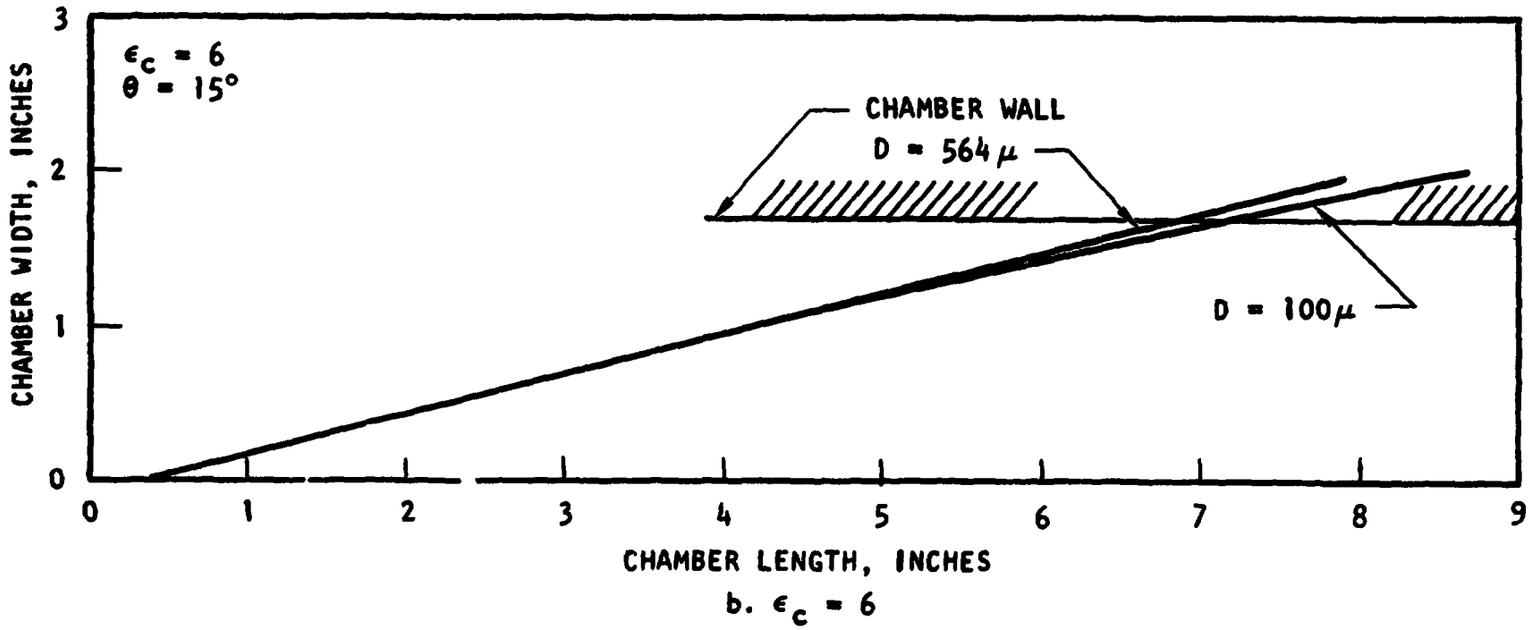

b. ϵ_c = 6

Figure 25. Predicted Droplet Trajectories for Chamber Gas Velocities Encountered With 200 F Initial Wax Temperature

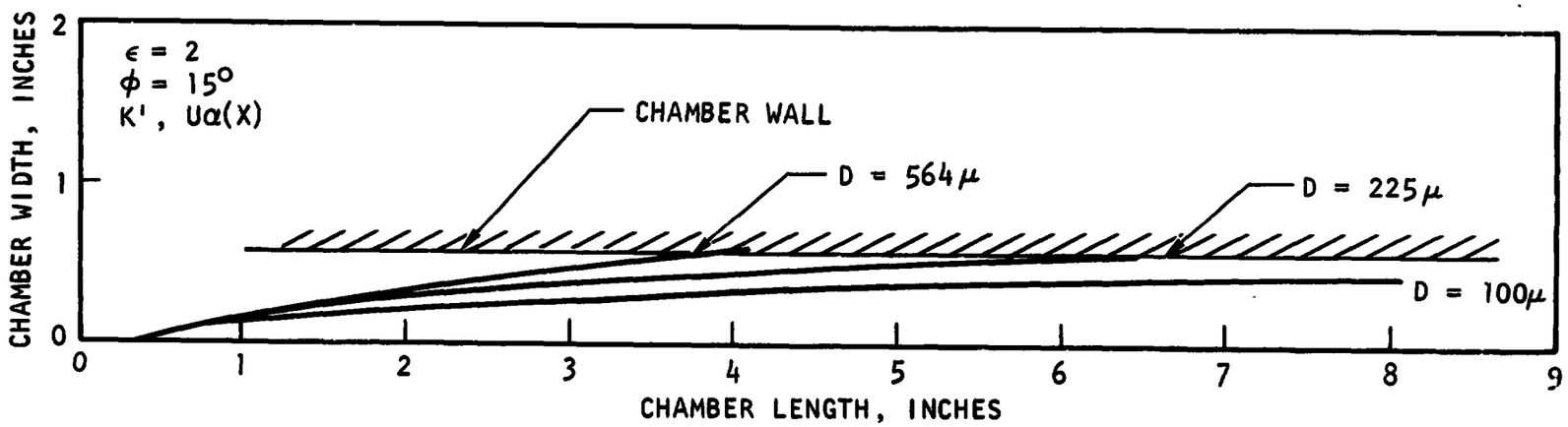

Figure 26. Predicted Droplet Trajectories for Chamber Gas Velocities Resulting With Heated Wax (~1585 F) Initial Temperature

The LISP model was utilized to determine quantitatively the relative amount of mass that would strike the walls if the gas velocity were zero. This prediction should be reasonably accurate for the contraction ratio of 2 configuration since little turning of the sprays is calculated to occur. In addition, due to some turning of the spray, these predictions will tend to over-estimate the amount of mass actually reaching the wall for a contraction ratio of 2. The chamber dimensions were superimposed over the mass profiles and the mass lying outside of this boundary was summed and divided by the total mass. In this way the percent mass striking the wall was estimated. LISP calculations were carried out for several chamber lengths and the results are shown in Fig. 27. Note that the initial location of mass striking the wall corresponds reasonably well with the location determined from LISP. It is obvious from this plot that considerable mass is likely to reach the wall for a contraction ratio of 2 before any significant vaporization or burning of the droplet occurs. From the above discussion it is felt that the occurrence of fuel impinging on the chamber wall precluded the ability to determine the effect of gross changes in gas velocity on dropsize.

In summary, the choice of the initial temperature of the wax (i.e., 200 F) did not take into consideration the large droplet heat-up times required to initiate vaporization. In general, normal propellants have only a 200 to 300 F temperature rise to initiate boiling. In the past, the resulting sensible heat rise necessary to initiate boiling has been included in the model by simply adjusting the overall vaporization rate. Due to the small percentage of total heat necessary and the short time requirements to bring the droplets to their boiling temperature, this technique was adequate. Due, however, to the large difference in ΔT (T_{boil}-$T_{initial}$) for the wax propellants, this approach cannot be taken. The inadequacy of this approach was not discovered until low hot-fire c* performance showed a large difference between the anticipated and actual results. Re-examining the combustion model formulation and possible explanations for the discrepancy between actual and anticipated c* performance, it was decided to run the droplet heating version of DER to see if the hot-fire results

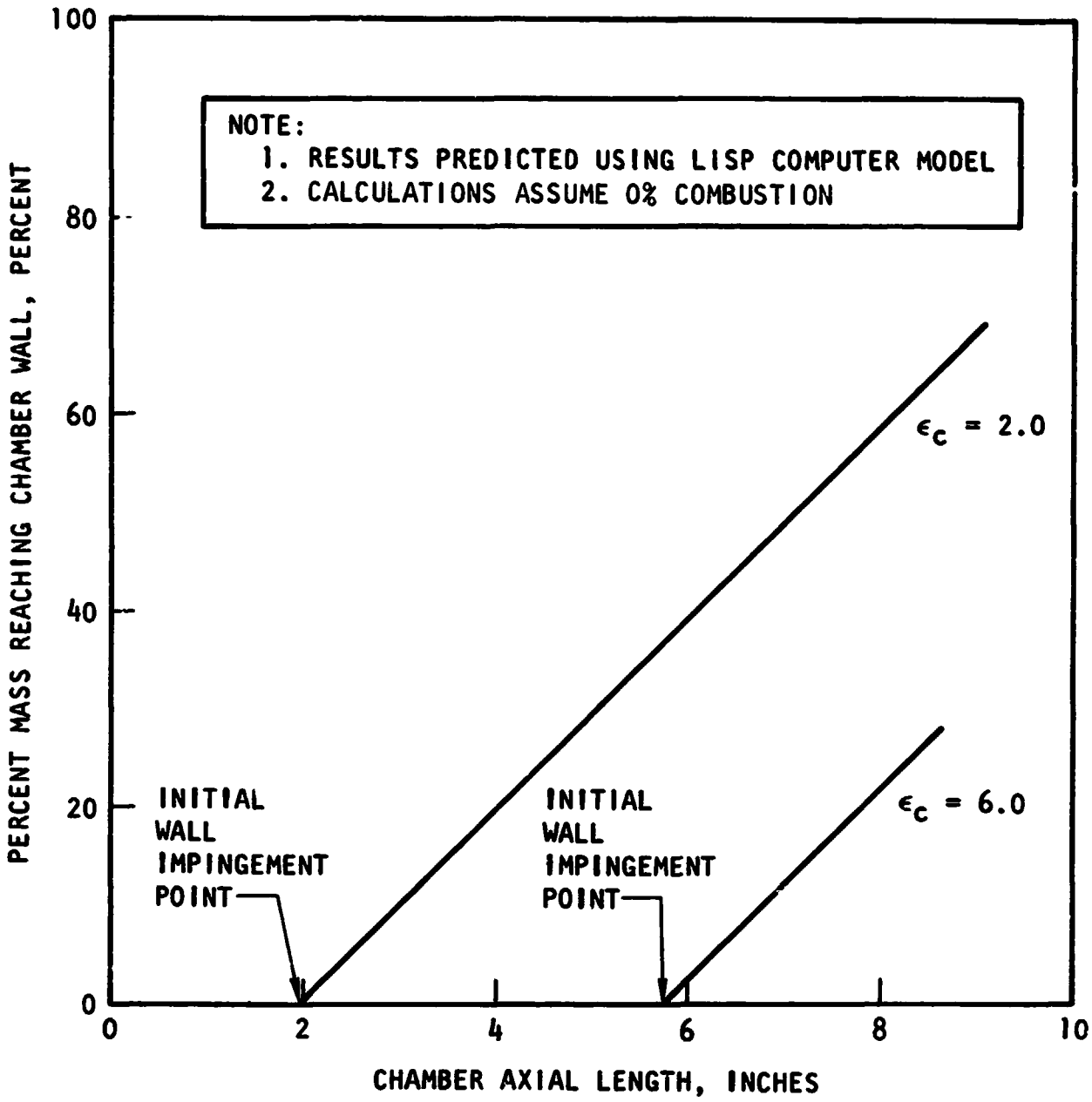

Figure 27. Percentage of Liquid (Wax) Mass Reaching Chamber Wall in the Absence of Axial Combustion Gas Velocity

could be explained. The results of this analysis, of course, clearly revealed that the c* performance was strongly influenced by the long droplet heat-up times. The subsequent effect on the initial vaporization rates, especially as it allowed substantial liquid wax impingement on the walls of the smaller width engine, masked the influence of the chamber gas velocity on atomization in the higher velocity region and therefore limits the overall range of this "proof of principle" study.

CONCLUSIONS AND RECOMMENDATIONS

Several conclusions can be drawn from the results: These are:

1. The experimental method used has yielded quantitative data that provide considerable new insight into rocket spray combustion processes.

    a. The vaporization characteristics calculated using the droplet heating version of the DER program compare well with hot firing data.

    b. The apparent dropsize obtained by comparing model calculations with experimental η_{c^*} data appears to be quantitatively correct, although an empirical correction for axial gas velocity effects is needed.

    c. Wax appears to offer excellent technique for checking the JANNAF combustion model formulation since the required input conditions of spray dropsize have been extensively studied. This removes the requirement for altering the cold-flow predicted dropsize to account for physical property effects.

2. The most useful data were obtained from tests at $\varepsilon_c = 6$. Data from $\varepsilon_c = 2$ tests were apparently contaminated by excessive wax spray impingement on the combustor wall. This resulted, in large measure, from the long droplet warm-up times.

3. Calculations suggest that preheating the wax to a higher temperature should sufficiently reduce the amount of wax striking the $\varepsilon_c = 2$ chamber walls so that gas velocity effects on atomization can be determined.

4. Another method would be to use another fuel that has a lower boiling temperature. This approach would eliminate the ability to have

an independent check on dropsize since dropsize measurements with the particular fluid may not exist. However, while the actual value of dropsize may not be measured the results from this program suggest that the model is sufficiently accurate so that differences in apparent dropsize based on model predictions and hot-fire data would be attributable to reduction of the zero gas velocity dropsize. Therefore, the relative effects of gas velocity on atomization could be determined over a larger range in velocity.

REFERENCES

1. AFRPL-TR-68-147: Correlation of Spray Injector Parameters With Rocket Engine Performance, Final Report, Rocketdyne, a division of North American Rockwell, Canoga Park, California, June 1968.

2. NASA CR-72487: Space Storable Propellant Performance Study, Final Report, Rocketdyne, a division of North American Rockwell, Canoga Park, California, November 1968.

3. Falk, A: Space Storable Propellant Performance Study Gas/Liquid Like-Doublet Injector Characterization, Final Report, Contract NAS3-12051, Rocketdyne, a division of North American Rockwell, Canoga Park, California, to be issued.

4. R-8455: Correlation of Spray Dropsize Distribution and Injector Variables, Rocketdyne, a division of North American Rockwell, Canoga Park, California, December 1971.

5. Hines, W., et al.: Development of Injector Chamber Compatability Analysis, Final Report, R-8048 (AFRPL-TR-70-12), Rocketdyne, a division of North American Rockwell, Canoga Park, California, July 1971.

6. Landis, R., W. Wagner, and W. Studhalter: "Experimental Heat Transfer Rates in Advanced Oxygen/Hydrogen Toroidal Thrust Chambers," 9th Liquid Propulsion Symposium, Vol. I, 25-27 October 1967 pp. 597-616.

7. Combs, L. P.: Liquid Rocket Performance Computer Model With Distributed Energy Release, Final Report (R-8888), Rocketdyne, a division of North American Rockwell, Canoga Park, California, June 1972.

8. Combs, L. P., et al.: Liquid Rocket Performance Computer Model With Distributed Energy Release (Documentation for Interim Delivery of the Revised Computer Program With Droplet Heating), (no report number), NASA Contract NAS7-746, Rocketdyne, a division of North American Rockwell, Canoga Park, California, 15 March 1971.

9. Allison, C. B.: Combustion of Shell 270 Wax as Droplets at High Temperature and Atmospheric Pressure, (no report number) Mechanical Engineering Department, The Pennsylvania State University, September 1971.

10. Reid, R. C. and Sherwood, T. K.: The Properties of Gases and Liquids, McGraw-Hill Book Co., New York (1958).

APPENDIX A: HEAT TRANSFER ANALYSES

During the past decade, Rocketdyne has done considerable experimental work in the area of combustion gas heat transfer. The effects of the chamber geometry, injector type, propellant combination, and chamber pressure have been extensively investigated. An analytical model has been developed utilizing experimental results that adequately predict the combustion gas convective film coefficient profile in a thrust chamber.

To compute the heat flux to the wall for a given allowable gas-side wall temperature (T_{wg}), both the driving temperature and the combustion gas heat transfer coefficient (h_g) must be determined. The combustion gas flow near the wall is retarded due to viscous effects resulting in a local temperature rise so that the local static temperature is not the proper driving potential for high-speed flow. The correct driving potential is referred to as the recovery or adiabatic wall temperature (T_{aw}) and is related to the combustion temperature (assumed to be the local stagnation temperature), in terms of the local Mach number as

$$T_{aw} = \left[\frac{1 + r\,\frac{\gamma-1}{2}\,M^2}{1 + \frac{\gamma-1}{2}\,M^2}\right] T_c \qquad \text{(A-1)}$$

where the recovery factor, r, for turbulent flow is given by

$$r = \sqrt[3]{N_{Pr}} \qquad \text{(A-2)}$$

For gases, since $N_{Pr} < 1$, the adiabatic wall temperature is always somewhat less than the combustion temperature with the maximum deviation occurring in the highest Mach number regions.

The combustion temperature (T_c) is corrected for incomplete combustion by the relation

$$T_c = T_{c_{ideal}} \cdot \eta_{c^*}{}^2 \qquad \text{(A-3)}$$

where η_{c^*} is the characteristic velocity efficiency.

Numerous analytical methods have been developed and presented in the literature for computing rocket motor gas-side heat transfer rates. With the present degree of sophistication of the high-speed digital computer, the solution of the proper boundary layer based equations is justified from a cost, accuracy, and manpower utilization standpoint. The allowance for intricate definition of the momentum and energy boundary layer development, and the study of the related viscous drag and heat rejection to the chamber walls in a parametric manner allows for improved nozzle and combustion chamber design.

The approach employed at Rocketdyne is similar to the methods of Elliot, Bartz, and Silver (Ref. A-1). The integral energy boundary-layer equation can be written in terms of the energy thickness, defined by the relation

$$\phi = \int_0^{\delta_T} \frac{\rho_u}{\rho_{u_\infty}} \left(1 - \frac{T_o - T_{wg}}{T_c - T_{wg}}\right) dy \qquad \text{(A-4)}$$

as

$$\frac{d\phi}{ds} = C_H \left[\frac{T_{aw} - T_{wg}}{T_c - T_{wg}}\right] - \phi\left[-\frac{1}{(T_c - T_{wg})} \frac{dT_{wg}}{ds} + \frac{1}{\rho_u} \frac{d(\rho_u)}{ds} + \frac{1}{R} \frac{dR}{ds}\right] \qquad \text{(A-5)}$$

This equation, which is in axisymmetric form, is uncoupled from the momentum equation. Solution requires an empirical relationship between the energy thickness and the local Stanton number. The relationship used, which was obtained initially by an analogy between the nondimensional heat transfer coefficient and the local skin friction coefficient, is for turbulent flow:

$$C_H = \frac{0.0122}{(Re_\phi)^{0.25}} \left(\frac{T_\infty}{T_r}\right) \left(\frac{\rho_\infty}{\rho_r}\right)^{1/4} \left(\frac{\mu_r}{\mu}\right)^{1/4} \frac{1}{N_{Pr}^{2/3}} \quad \text{(A-6)}$$

The reference properties in this equation are usually evaluated at the Eckert reference temperature defined as:

$$T_r = T_c + 0.50\ (T_c - T_s) + 0.22\ (T_{aw} - T_s) \quad \text{(A-7)}$$

Simultaneous solution of Eq. 5 and 6 to yield local energy thicknesses and corresponding Stanton number values requires (in addition to combustion gas properties), (1) knowledge of the point of flow attachment (i.e., point of stable boundary-layer initiation) and (2) the initial energy thickness or Stanton number at that point. These latter two items require reliance on experimental data. It has been determined empirically, for example, that in a thrust chamber the boundary layer is unlikely to begin to grow in a cumulative fashion until encountering a favorable pressure gradient (converging walls). This is depicted schematically in Fig. A-1. In a region of weak or adverse pressure gradient the boundary-layer flow is easily disrupted due to pressure fluctuations, turbulence level, or recirculation phenomenon. In this region, the injector design can strongly influence the heat transfer rates.

The initial Stanton number at the point of flow attachment has been experimentally determined at Rocketdyne as a function of local combustion gas mass flux for a range of chamber contraction ratios. These results are shown in Fig. A-2. For high-thrust chambers, where boundary layer development lengths are relatively long, the solution in the throat region is fairly insensitive to attachment value. In the case of small combustors (L < 6 inches) accurate estimates of both the point of flow attachment and initial Stanton number are essential to reliable combustion gas heat transfer prediction.

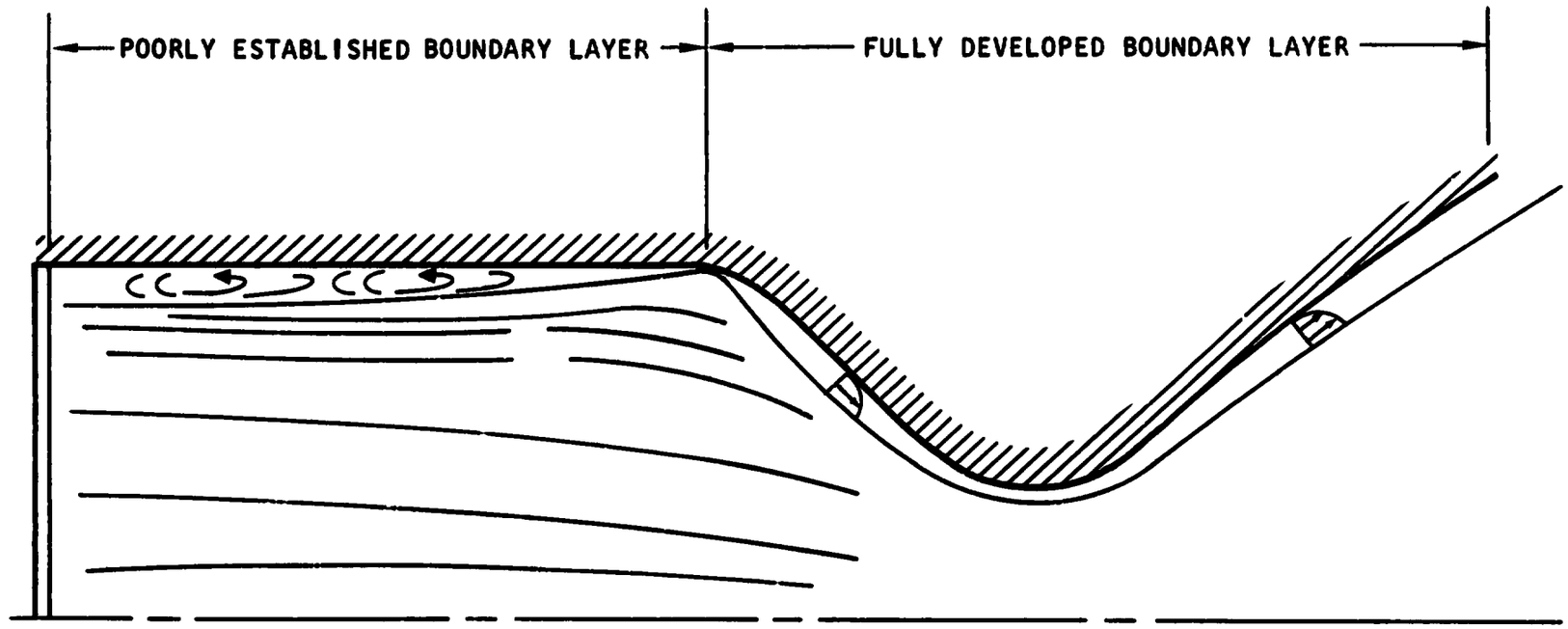

Figure A-1. Combustion Chamber Boundary Layer Behavior

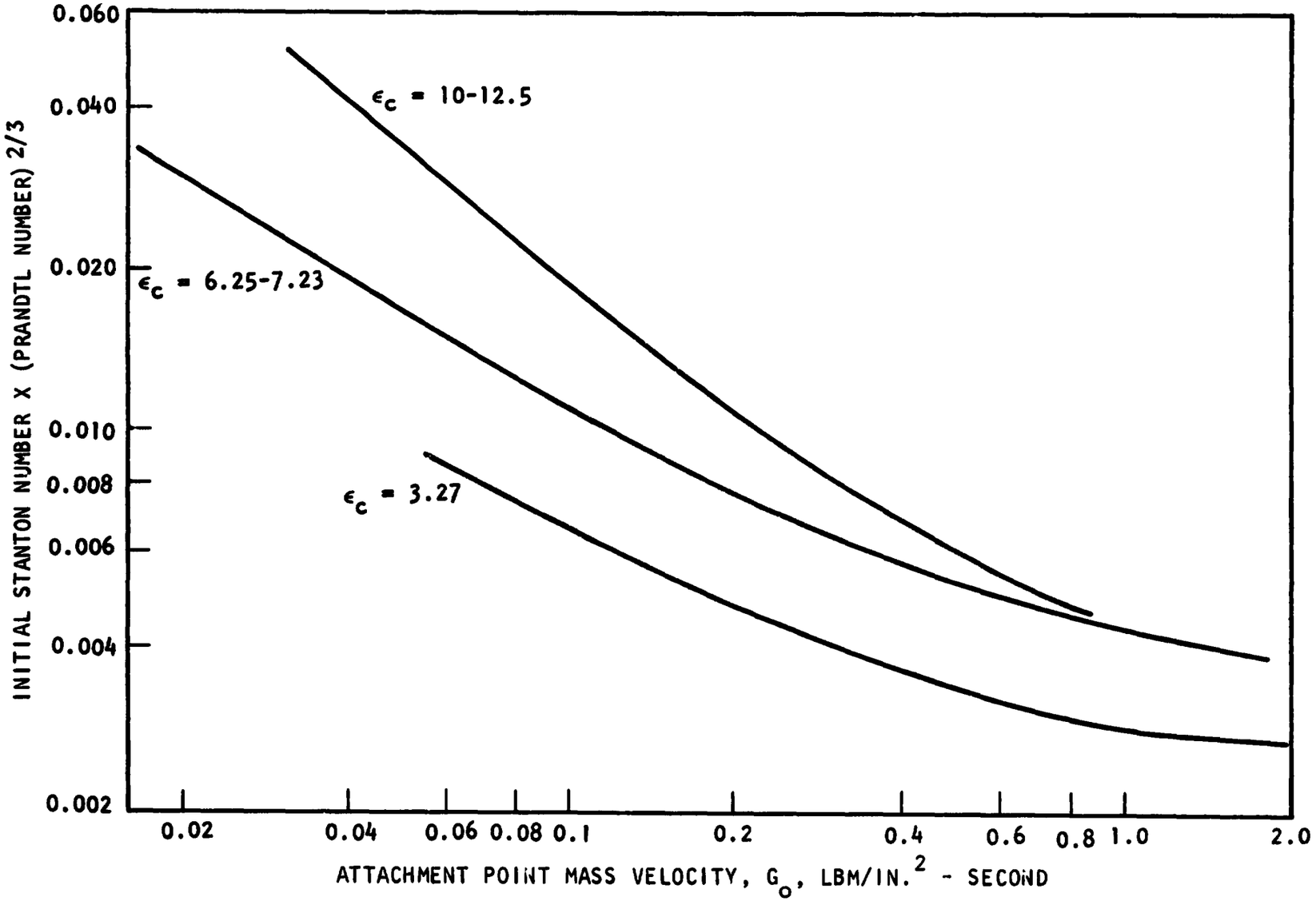

Figure A-2. Initial Stanton-Prandtl Parameter at Boundary Layer Attachment Point

These results were used to specify the conditions necessary for solution of the heat transfer equations discussed above. Solutions were obtained over a range of c* performance and chamber length for each contraction ratio (2 and 6). The results are presented in Fig. A-3. The ordinate of these plots use Σ Q/A which represents the total heat loss over the entire engine.

REFERENCES

A-1. Elliot, D. G., D. R. Bartz, and S. Silver: Calculation of Turbulent Boundary Layer Growth and Heat Transfer in Axisymmetric Nozzles, Report No. 32-387, Jet Propulsion Laboratory, Pasadena, California, February 1963.

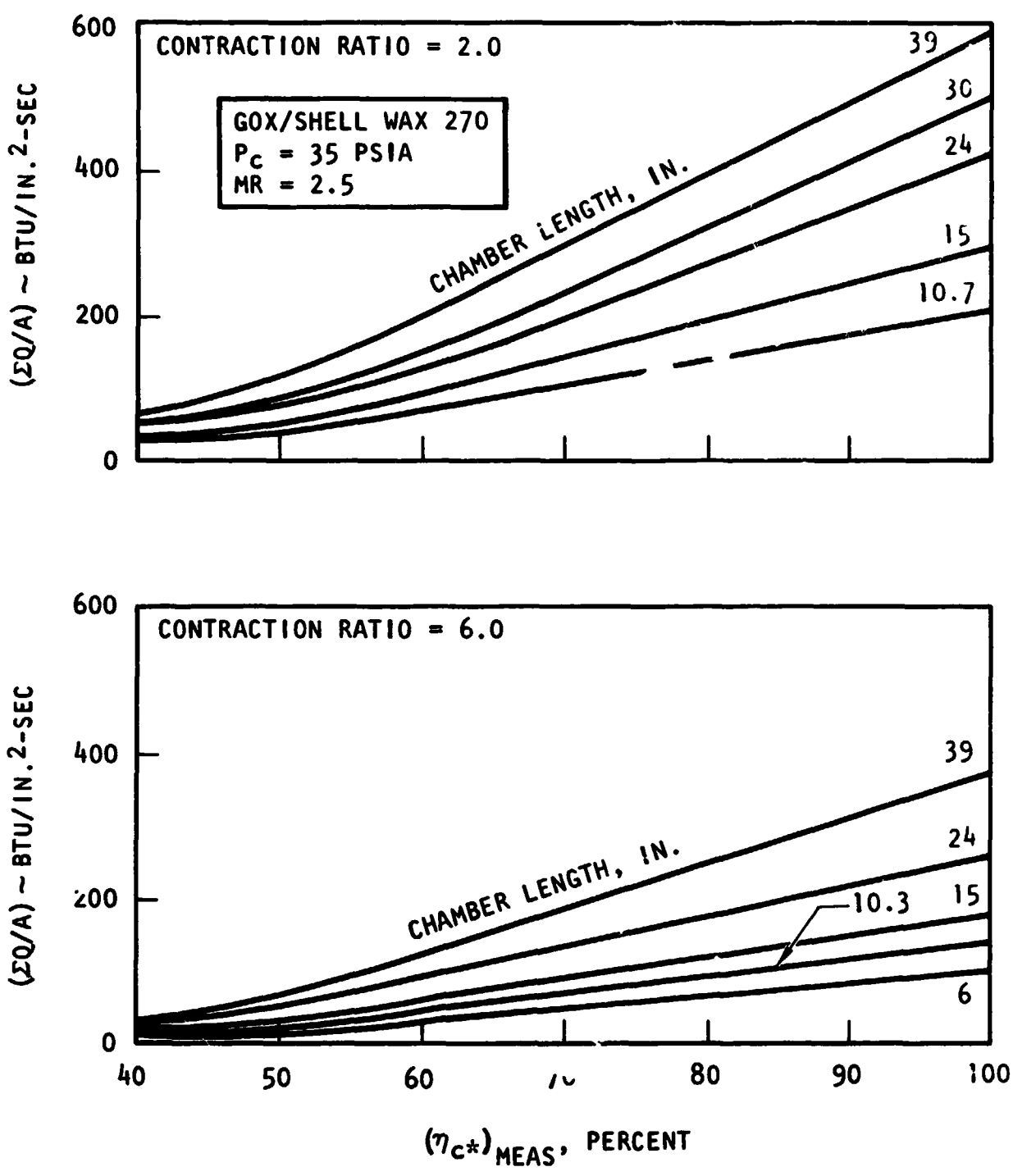

Figure A-3. Total Head Loss as a Factor of η_{c*} for Several Chamber Lengths

UNCLASSIFIED

Security Classification

DOCUMENT CONTROL DATA - R & D

(Security classification of title, body of abstract and indexing annotation must be entered when the overall report is classified)

1 ORIGINATING ACTIVITY *(Corporate author)*

ROCKETDYNE
a division of North American Rockwell Corporation
6633 Canoga Avenue, Canoga Park, California 91304

2a. REPORT SECURITY CLASSIFICATION

UNCLASSIFIED

2b. GROUP

3 REPORT TITLE

Study of Spray Disintegration in Accelerating Flow Fields

4 DESCRIPTIVE NOTES *(Type of report and inclusive dates)*

Final Report

5 AUTHOR(S) *(First name, middle initial, last name)*

W. H. Nurick

6 REPORT DATE	7a. TOTAL NO. OF PAGES	7b. NO. OF REFS
June 1972	100	10

8a. CONTRACT OR GRANT NO.	9a. ORIGINATOR'S REPORT NUMBER(S)
NAS2-6494	R-9017
b. PROJECT NO.	
c.	9b. OTHER REPORT NO(S) *(Any other numbers that may be assigned this report)*
d.	NASA CR 114479

10 DISTRIBUTION STATEMENT

11. SUPPLEMENTARY NOTES	12. SPONSORING MILITARY ACTIVITY
	Jet Propulsion Laboratory Pasadena, California NASA

13 ABSTRACT

An analytical and experimental investigation was conducted to perform "proof of principle" experiments to establish the effects of propellant combustion gas velocity on propellant atomization characteristics. The propellants were gaseous oxygen (GOX) and Shell Wax 270. The fuel was thus the same fluid used in earlier primary cold-flow atomization studies using the frozen wax method. Experiments were conducted over a range in L* (30 to 160 inches) at two contraction ratios (2 and 6). Characteristic exhaust velocity (c*) efficiencies varied from 50 to 90 percent. The hot-fire experimental performance characteristics at a contraction ratio of 6.0 in conjunction with analytical predictions from the droplet heat-up version of the Distributed Energy Release (DER) combustion computer program showed that the apparent initial dropsize compared well with cold-flow predictions (if adjusted for the gas velocity effects). The results also compared very well with the trend in performance as predicted with the model. Significant propellant wall impingement at the contraction ratio of 2.0 precluded the determination of gross changes in gas velocity on dropsize.

DD FORM 1 NOV 65 1473

UNCLASSIFIED

Security Classification

14 KEY WORDS	LINK A		LINK B		LINK C	
	ROLE	WT	ROLE	WT	ROLE	WT
Combustion						
Mixing						
Dropsize						
Combustion models						